Synthesis and Properties of Liquid Crystalline Polyacetylenes with Different Spacer Lengths and Bridge Orientations

Jacky W. Y. Lam, Xiangxing Kong, Yuping Dong, Kevin K. L. Cheuk, Kaitian Xu, and Ben Zhong Tang*

Department of Chemistry and Center for Display Research, Hong Kong University of Science & Technology, Clear Water Bay, Kowloon, Hong Kong, China

Received December 14, 1999; Revised Manuscript Received April 13, 2000

ABSTRACT: A group of mesomorphic polyacetylenes with different lengths of alkyl spacer −{HC═C[$(CH_2)_m$−OCO−Biph−OC_7H_{15}]}$_n$− [**1**(*m*), *m* = 2, 3, 4, 9] and orientations of ester bridge −{HC═C[$(CH_2)_3$−CO_2−Biph−OC_7H_{15}]}$_n$− [**2**(3)] are synthesized, and the effects of the structural variables on the properties of the polymers are investigated. The liquid crystalline acetylene monomers *n*-{[(4′-heptoxy-4-biphenylyl)oxy]carbonyl}-1-alkynes **3**(*m*) and 5-{[(4′-heptoxy-4-biphenylyl)carbonyl]oxy}-1-pentyne **4**(3) are prepared by consecutive etherification and esterification reactions. The T_m and T_i values of **3**(*m*) decrease with an increase in the spacer length (*m*). While **3**(3) shows a monotropic SmA phase, its counterpart with a different ester orientation **4**(3) exhibits an enantiotropic SmB phase. The monomers are polymerized by transition-metal halides and carbonyls, and the polymerizations catalyzed by WCl_6−Ph_4Sn under optimal conditions produce polymers with high molecular weights (up to 1.2×10^5) in high yields (up to 92%). The structures and properties of the polymers are characterized and evaluated by IR, UV, TGA, DSC, POM, and XRD analyses. With the increase in the spacer length, the thermal stability of the polymers increases, their T_g and T_i decrease, and the packing arrangements in their mesophases change from mixed mono- and bilayer structures to a homogeneous monolayer structure. Compared to **1**(3), **2**(3) shows a blue-shifted absorption spectrum ($\Delta\lambda_{max}$ >30 nm), a higher T_g and T_i (ΔT ∼40 °C), and a better packed SmA_d structure.

Introduction

Liquid crystals are quintessential molecular electronics materials for the modern optical display technologies.[1] Conjugated polymers offer attractive possibilities for technological innovations,[2] and recent research efforts have been devoted to the exploration of their potential for use as thin film transistors,[3] light-emitting diodes,[4] and organic lasers.[5] Fusing the two components into one system, that is, attaching liquid crystalline pendants to conjugated polymer backbones, may lead to the development of new multifunctional organic materials potentially capable of enhancing existing, and creating novel, electronic and optical properties. Indeed, liquid crystalline conjugated polymers have been found, for example, to exhibit linearly[6] or circularly polarized emission[7] and have been utilized to impart new features to electrochromism.[8] Many technological applications proposed for liquid crystalline polymers, such as information storage[9] and nonlinear optics,[10] require high glass transition temperatures (T_g's).[11,12] Liquid crystalline conjugated polymers are promising candidate materials for such applications because conjugated polymers normally possess high T_g's,[13] thanks to the restricted segmental movements of the rigid polymer backbones.[14]

Attracted by the application perspective, many research groups have worked on the development of liquid crystalline conjugated polymers.[6−8,15,16] Polyacetylenes are archetypal conjugated polymers, but research on mesomorphic polyacetylenes is still in its infancy with only a few examples of such polymers being documented in the literature. Akagi and Shirakawa, for example, synthesized a group of liquid crystalline poly(1-pentynes), in which the polyalkyne main chain and the phenylcyclohexylyl or biphenylyl mesogens are bridged through an ether functionality.[15b,17] The Japanese group successfully aligned the polymers with a magnetic field and observed large electrical anisotropy ($\sigma_{||}/\sigma_{\perp}$ up to 10^5) of the aligned iodine-doped liquid crystalline polyacetylene films. Nuyken and co-workers incorporated biphenylyl mesogens with different spacer lengths to poly(1-propyne) (or polypropargyl) structure, again through an ether bridge.[18] Unfortunately, however, the polypropargyl derivatives were insoluble. The intractability poses a formidable obstacle in the purification and characterization of the polymers and significantly limits the scope of their practical applications. The mesophases of the polymers could not be assigned unambiguously, which makes the evaluation of their structure−morphology−property relationships a difficult proposition.

The limitation on the variety of liquid crystalline polyacetylenes is mainly due to the synthetic difficulty. The design of molecular structures of mesogen-containing acetylene monomers unavoidably involves the use of functional bridges to link the mesogenic and acetylenic moieties together (Chart 1). The functional groups have, however, often been found to deactivate the transition-metal catalysts used in the acetylene polymerizations. We have recently developed a variety of functionality-tolerant and air- and moisture-stable catalyst systems, some of which can even initiate acetylene polymerizations in water in the air.[19] With the success in the catalyst development, we have synthesized a large number of substituted polyacetylenes containing sugars, menthols, amino acids, crown ethers, oligo(ethylene glycol), and mesogenic pendants with ether, ester, amide, and cyano functionalities.[20−24] However, our initial attempt to investigate the liquid crystallinity

* To whom correspondence should be addressed. Telephone: +852−2358−7375. Fax: +852−2358−1594. E-mail: tangbenz@ust.hk.

10.1021/ma992097j CCC: $19.00
Published on Web 06/22/2000

Chart 1

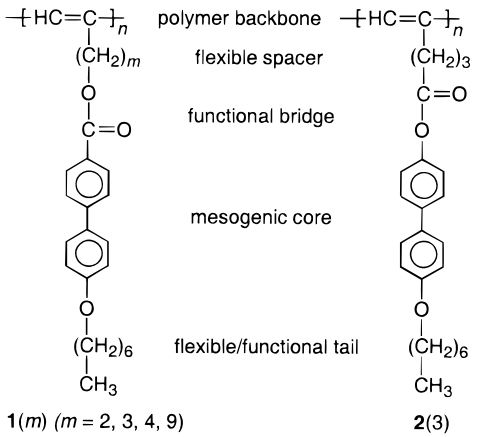

Chart 2

Liquid Crystalline Polyacetylenes $-[HC{=}C(LC)]_n-$

LC: flexible spacer +	functional bridge +	mesogenic core +	flexible or functional tail	
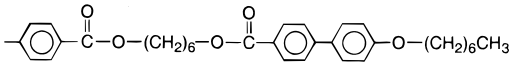				5
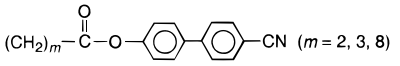				6
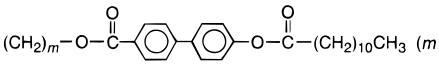				7
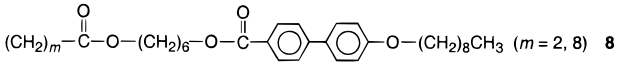				8
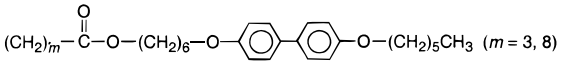				9
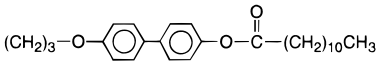				10
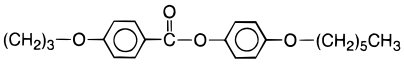				11
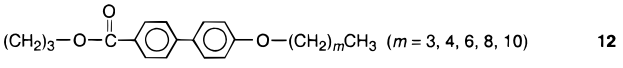				12
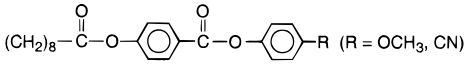				13

of a group of mesogen-containing poly(phenylacetylene) derivatives, poly({4-[({*n*-[(4′-cyano-4-biphenylyl)oxy]-alkyl}oxy)carbonyl]phenyl}acetylenes) (n = 6, 12), unfortunately failed.[19d] The nonmesomorphism of the polymers is probably due to the high rigidity of the poly(phenylacetylene) backbone coupled with the strong interaction between the highly polar *p*-cyanobiphenylyloxy pendants. By fine-tuning the backbone rigidity and pendant interaction through molecular engineering endeavor, we eventually succeeded in the development of liquid crystalline polyacetylenes with both poly(arylacetylene) (**5**)[20a] and poly(alkylacetylene) or poly(1-alkyne) (**6**)[19c] skeleton structures (Chart 2).

Because of the ease in their synthesis, we prepared a wide variety of poly(1-alkyne) derivatives containing different flexible spacers, functional bridges, mesogenic cores, and flexible or functional tails (**1**, **2**, **5**−**13**). We systematically studied their liquid crystalline properties and discovered some unique mesomorphic structures originating from the synergistic interplay of the rigid

Scheme 1

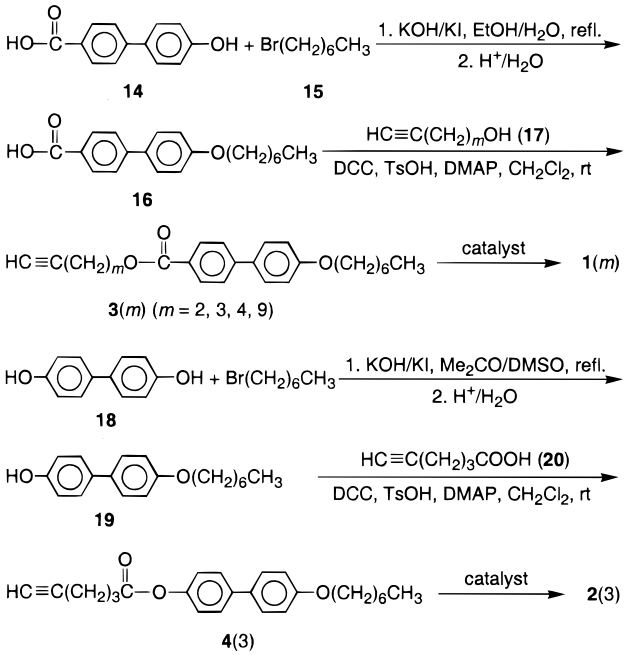

polymer backbone and the mesogenic pendants, including rotation-induced high-strength disclinations, shear-induced inversion walls, and solidification-induced parallel bands.[21a] We further found that the polyacetylenes are also luminescent[22] and photoconductive[23a] and demonstrated that their luminescence and photoconductivity can be modulated by electrical field and thermal perturbation.[24a] The mesogen-containing polyacetylenes are thus a group of new polymers with novel material properties, and it is of interest to investigate the effects of the molecular structures on the morphologies and properties of the polymers. In this paper, we report the synthesis and properties of the liquid crystalline polyacetylenes with different spacer lengths [**1**(*m*)] and bridge orientations [**1**(3) vs **2**(3)]. We found that both the spacer length and the bridge orientation affected the electronic transition, thermal stability, and packing arrangement of the mesomorphic polyacetylenes.

Results and Discussion

Synthesis and Mesomorphism of Monomers. We designed molecular structures of a group of mesogenic alkynes with different lengths of methylene spacers [**3**(*m*)] and elaborated a two-step reaction route for their synthesis (Scheme 1). We first etherified 4′-hydroxy-4-biphenylcarboxylic acid with 1-bromoheptane and then esterified the resultant acid (**16**) with *n*-alkyn-1-ol (**17**) in the presence of 1,3-dicyclohexylcarbodiimine (DCC), *p*-toluenesulfonic acid (TsOH), and 4-(dimethylamino)-pyridine (DMAP). We also designed and synthesized 5-{-[(4′-heptoxy-4-biphenylyl)oxy]carbonyl}-1-pentyne [**4**(3)], a closely related compound of **3**(3) with a different orientation of the ester bridge, again through a two-step etherification and esterification reaction route. All the intermediate and final products were thoroughly purified and fully characterized, and satisfactory analysis data were obtained (detailed spectroscopic data for the key intermediates and for all the monomers being given in the Experimental Section).

The acetylene monomers are crystalline at room temperature but show liquid crystallinity at high tem-

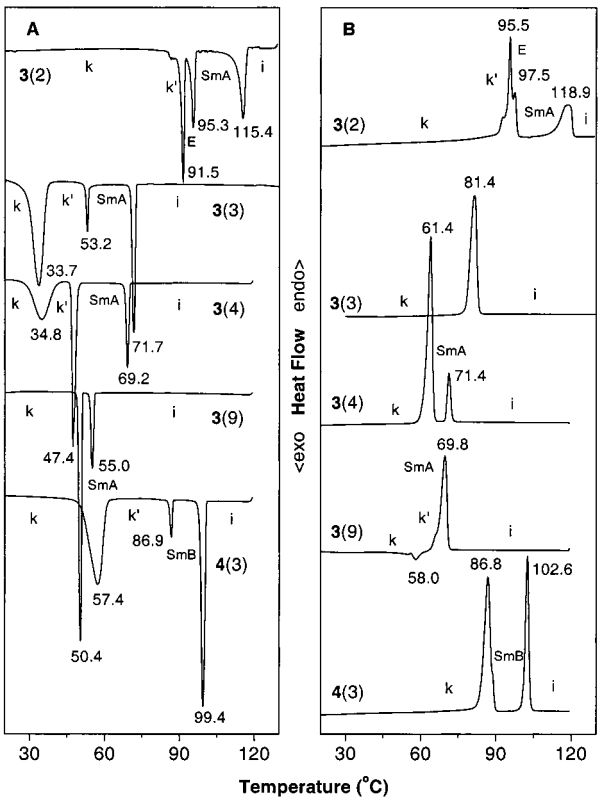

Figure 1. DSC thermograms of monomers **3**(*m*) (*m* = 2, 3, 4, 9) and **4**(3) recorded under nitrogen during the (A) first cooling and (B) second heating scans at a scan rate of 10 °C/min.

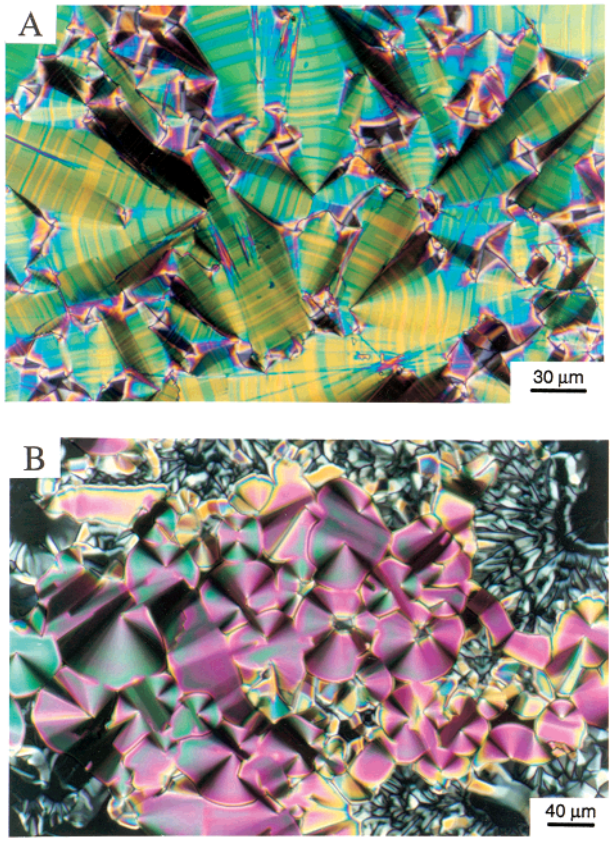

Figure 2. Polarized optical microphotographs of (A) **3**(2) at 93.6 °C (paramorphotic arced or banded focal-conic fan texture of crystal E phase) and (B) **4**(3) at 98.0 °C (mossy mosaic texture of SmB phase).

peratures. The thermotropic mesomorphism of the monomers was investigated by a combination of differential scanning calorimetry (DSC) and polarized optical microscopy (POM). The DSC thermograms of the monomers are shown in Figure 1, while two examples of their POM textures are given in Figure 2.

In the first cooling scan of **3**(2), three sharp peaks appear at 115.4, 95.3, and 91.5 °C, and a small exothermic shoulder occurs at 87.1 °C (Figure 1A). The DSC thermogram recorded in the second heating scan exhibits three overlapping peaks at ∼95 °C plus a separate peak at 118.9 °C. POM observation reveals that upon cooling from the isotropic state to 112 °C, a focal-conic fan texture corresponding to a smectic A phase emerges. Further cooling to 93.6 °C leads to the formation of *stable* and *continuous* concentric lines or arcs running across the backs of the fans (Figure 2A). Of the different types of mesophases evolved from the SmA phase, concentric arcs can only be observed in smectic B and crystal E and G phases.[25] The arcs formed at a SmA-to-SmB transition are transitory in nature: once the phase transition completes, the arcs disappear. The arcs in the crystal G phase formed on cooling SmB phase are broken; that is, they are not continuous from one fan area to another but show breaks. On the other hand, the arcs in the crystal E phase are not transitory but remain throughout the temperature range in which the phase persists.[25] It thus becomes clear that the crystal E phase has formed at ∼94 °C, the formation of whose arcs is probably caused by the different contraction directions of the layer ordering at the SmA−E transition. The monomer solidifies at ∼92 °C. The small exothermic peak at ∼87 °C may be associated with crystal transformation from one state to another (k−k transition); such polymorphism has often been observed in our mesogen-containing acetylene monomers, regardless of whether they are liquid crystalline or not.[21a,b] Reheating **3**(2) regenerates the paramorphotic crystal E and SmA textures in sequence; that is, the mesomorphism is enantiotropic.

The monomer with three methylene spacers [**3**(3)] shows three exothermic peaks at 71.7, 53.2, and 33.7 °C during the first cooling scan (Figure 1A). Cooling **3**(3) from the isotropic state to 70.5 °C results in the formation of typical focal-conic fan textures of SmA phase. The monomer solidifies at ∼54 °C, and the exothermic peak at 33.7 °C thus should be associated with a k−k transition. The crystal−crystal and liquid crystal transitions are, however, monotropic, as the DSC thermogram recorded in the second heating scan only displays an isotropization peak at 81.4 °C.

The DSC thermogram of **3**(4) shows three transition peaks at 69.2, 47.4, and 34.8 °C in the first cooling cycle. With the aid of POM, the peak at 69.2 °C is assigned with ease to the transition from the isotropic state to the SmA phase, because typical focal-conic fan textures readily form when the monomer is cooled to below this transition temperature. The SmA textures can be observed during both heating and cooling scans; the liquid crystalline transition is thus enantiotropic in nature.

Two transition peaks are detected at 55.0 and 50.4 °C by the DSC analysis of **3**(9) in the cooling cycle. The mesophase in this temperature region (50−55 °C) is identified to be SmA by the POM observation (typical focal-conic fan texture). Further cooling leads to solidification. Interestingly, a small exothermic peak is detected by DSC at 58.0 °C during the second heating

Table 1. Thermal Transitions and Corresponding Thermodynamic Parameters of 3(*m*) and 4(3)[a]

		T, °C [Δ*H*, kJ/mol; Δ*S*, J/(mol K)]	
no.	monomer	cooling	heating
1	**3**(2)	i 115.4 (−8.35; −21.49) SmA 95.3 (−4.32; −11.72) E 91.5 (−7.16; −19.63) k′ 87.1 (−) k	k 92.7 (−) k′ 95.5 (−) E 97.5 (14.01; 37.80)[b] SmA 118.9 (9.39; 23.95) i
2	**3**(3)	i 71.7 (−6.79; −19.69) SmA 53.2 (−1.72; −5.27) k′ 33.7 (−17.23; −56.15) k	k 81.4 (39.04; 110.11) i
3	**3**(4)	i 69.2 (−6.47; −18.90) SmA 47.4 (−15.66; −48.85) k′ 34.8 (−16.86; −54.75) k	k 64.1 (35.81; 106.18) SmA 71.4 (6.41; 18.60) i
4	**3**(9)	i 55.0 (−6.12; −18.65) SmA 50.4 (−20.34; −62.86) k	k 58.0 (−5.04; −15.22) k′ 65.3 (−) SmA 69.8 (60.75; 177.13)[b] i
5	**4**(3)	i 99.4 (−18.38; −49.33) SmB 86.9 (−2.41; −6.69) k′ 57.4 (−27.85; −84.25) k	k 86.8 (30.31; 84.20) SmB 102.6 (18.88; 50.24) i

[a] Data taken from the DSC thermograms recorded under an atmosphere of dry nitrogen in the first cooling and second heating scans; abbreviations: k = crystalline state, Sm = smectic phase, i = isotropic liquid. [b] Sum of overlapping transitions.

scan. This is undoubtedly due to the crystallization of the monomer. As temperature increases, the crystal packing transforms to a better ordered subphase, thus releasing heat to the surrounding.[26] POM observation reveals that the big endothermic peak at ∼70 °C actually involves two transitions: a crystal-to-SmA transition followed by the isotropization of the SmA phase. The monomer shows a large degree of supercooling (∼15 °C). This is not uncommon for mesogen-containing acetylene monomers; for example, the degrees of supercooling for the monomers of **13** are even larger, being 17 and 41 °C when the tails are respectively cyano and methoxy groups.[21a]

The monomer **4**(3) is a structural isomer of **3**(3) with a different orientation of the ester bridge, and it is of interest to check how it behaves mesomorphically. During the first cooling cycle, **4**(3) shows three exotherms at 99.4, 86.9, and 57.4 °C (Figure 1A). When the isotropic liquid is cooled to 98 °C, mosaic textures with fans and mosses are observed (Figure 2B). These unique paramorphotic textures are diagnostic of an i−SmAB transition, that is, formation of SmB phase from the isotropic liquid via a very narrow SmA phase. The fan texture starts to form normally in the SmA phase, but as it develops, it goes through the transition to the SmB phase that prefers to adopt a mosaic texture. No transition bars are observed during the A−B phase change, and close inspection of the microphotograph shown in Figure 2B reveals that many of the mosaic textures are composed of pseudo focal-conic fans with smooth surfaces, suggesting that the SmB phase is hexatic in nature.[25] The mossy areas may be generated by the nucleation from the isotropic liquid directly to the SmB structure.[25,27]

In the second heating cycle, two transition peaks appear at 86.8 and 102.6 °C, which are respectively identified as k−SmB and SmAB−i transitions by POM observations. Blumstein et al. prepared a similar acetylene monomer with a methoxy tail, which shows a monotropic nematic phase.[28] In contrast, our monomer with a heptoxy tail exhibits a better ordered enantiotropic smectic B phase. Thus, the tail length greatly affects the mesomorphic properties of the acetylene monomers. According to Gray and co-workers, extension of the tail length may enhance SmB packing arrangements,[29] which is proved to be the case in our system. Comparing the mesomorphic properties of **4**(3) and **3**(3), it is clear that the different linkage order of the ester bridge between the mesogenic core and the flexible spacer brings about dramatically different mesomorphism: **4**(3) shows the enantiotropic SmB phase, while its counterpart **3**(3) exhibits the monotropic SmA phase.

Table 1 summarizes the thermodynamic parameters associated with the mesomorphic transitions of the acetylene monomers. All the SmA, SmB, and crystal E transitions are characterized by large enthalpy (Δ*H*) and entropy changes (Δ*S*), confirming that these transitions are first order in nature[10] and suggesting that liquid crystal dimers are acting as virtual mesogenic units.[12,40] Two acetylene monomers may form a dimer through hydrogen bonding between the acidic acetylene hydrogen (═C−*H*) and the electron-withdrawing carbonyl oxygen (C═*O*) in a head-to-tail antiparallel interdigitating fashion. Such dimer species are bulky in volume and anisotropic in shape, whose packing/disassembling would involve a large change in the order of the system, thus giving the observed unusually large Δ*S* values.[12,21a]

Although the monomers **3**(*m*) show different polymorphisms and mesophases, the melting (T_m) and isotropization temperatures (T_i) generally decrease with the increase in the spacer length, probably due to the plasticization effect of the long alkyl spacers. Interestingly, while structurally similar, **3**(3) and **4**(3) behave strikingly different, with the latter showing better packing order and higher transition temperatures. Thus, although the change in the orientation of the ester bridge looks like a subtle structural variation, it does significantly alter the thermal and mesomorphic properties of the acetylenic liquid crystals.

Polymerization Reactions. Mo- and W-based catalysts are the most widely used "classic" initiators for acetylene polymerizations.[19,30] The catalyst systems have, however, often been found to be incapable of polymerizing acetylene monomers with functional groups. In our previous work, for example, we found that neither $MoCl_5$− nor WCl_6−Ph_4Sn was an effective catalyst for the polymerization of HC≡CC_6H_4-*p*-$CO_2(CH_2)_6OCO$−Biph−$O(CH_2)_6CH_3$ (**21**), an acetylene monomer with both ester and ether functionalities.[20a] Monomers **3**(*m*) and **4**(3) structurally resemble **21**, and their polymerizations could be difficult. Delightfully, however, by optimizing the reaction conditions, we succeeded in polymerizing the functional acetylene monomers to high molecular weight polymers using the classic Mo and W catalysts.

Table 2 lists the polymerization results of **3**(2). WCl_6 alone in dioxane gives a very low polymer yield (7.5%). When Ph_4Sn is used as a cocatalyst, the yield increases to 18.8% and the weight-average molecular weight (M_w) also increases. Much higher yield (72.4%) and M_w (40 800) are obtained when the polymerization temperature is raised to 60 °C. When the solvent is changed from dioxane to toluene, the yield at room temperature is improved but the M_w largely decreases (cf., Table 2,

Table 2. Polymerization of 4-{[(4′-Heptoxy-4-biphenylyl)carbonyl]oxy}-1-butyne [3(2)][a]

no.	catalyst	solvent	temp (°C)	yield (%)	M_w[b]	M_w/M_n[b]
1	WCl_6	dioxane	rt[c]	7.5	15200	1.75
2	WCl_6-Ph_4Sn	dioxane	rt	18.8	37400	2.06
3	WCl_6-Ph_4Sn	dioxane	60	72.4	40800	2.22
4	WCl_6-Ph_4Sn	toluene	rt	36.3	7800	1.30
5	WCl_6-Ph_4Sn	toluene	60	51.6	17100	1.55
6	$MoCl_5-Ph_4Sn$	dioxane	rt	27.4	74100	3.23

[a] Carried out under a dry atmosphere of nitrogen for 24 h; $[M]_0$ = 0.2 M, [cat.] = ([cocat.] =) 10 mM. [b] Determined by GPC in THF on the basis of a polystyrene calibration. [c] rt = room temperature.

Table 3. Polymerization of 5-{[(4′-Heptoxy-4-biphenylyl)carbonyl]oxy}-1-pentyne [3(3)][a]

no.	catalyst[b]	solvent	temp (°C)	yield (%)	M_w[c]	M_w/M_n[c]
1	WCl_6	dioxane	rt[d]	18.9	52000	2.22
2	WCl_6-Ph_4Sn	dioxane	rt	90.7	122700	4.09
3	WCl_6-Ph_4Sn	dioxane	40	84.2	74770	2.38
4	WCl_6-Ph_4Sn	dioxane	60	85.2	49900	2.25
5	WCl_6-Ph_4Sn	dioxane	80	76.9	29400	1.82
6	WCl_6-Ph_4Sn	toluene	60	48.0	8800	1.29
7	$MoCl_5-Ph_4Sn$	dioxane	60	12.1	11800	1.90
8	$W(mes)(CO)_3$	CCl_4	60	36.0	16400	1.58
9	$Mo(nbd)(CO)_4$	CCl_4	60	38.1	11900	1.38

[a] Carried out under a dry atmosphere of nitrogen for 24 h; $[M]_0$ = 0.2 M, [cat.] = ([cocat.] =) 10 mM. [b] Abbreviations: mes = mesitylene, nbd = 2,5-norborndiene. [c] Determined by GPC in THF on the basis of a polystyrene calibration. [d] rt = room temperature.

nos. 4 and 2). In this solvent, increasing the polymerization temperature again leads to increments in both yield and M_w. $MoCl_5-Ph_4Sn$ gives a polymer with a high molecular weight albeit in a relatively low yield (Table 2, no. 6). This result is somewhat surprising because we have so far not been able to polymerize any acetylene monomers with *ester* functionality using the Mo catalyst,[19] although Akagi and Shirakawa have reported that $MoCl_5-Ph_4Sn$ is an effective catalyst for the polymerizations of their functional acetylene monomers containing *ether* moieties.[17]

The effects of catalyst, cocatalyst, solvent, and temperature on the polymerization of **3**(3) are summarized in Table 3. Similar to that of **3**(2), polymerization of **3**(3) by WCl_6 in dioxane gives a low polymer yield. Addition of Ph_4Sn dramatically boosts both the yield and M_w of the polymer (Table 3, no. 2). Increasing the polymerization temperature generally leads to decrements in both yield and M_w, which is different from the trend observed in the polymerization of **3**(2). $MoCl_5-Ph_4Sn$ can also polymerize **3**(3) but again in low yield. Metal carbonyl complexes $W(mes)(CO)_3$ and $Mo(nbd)(CO)_4$ are air- and moisture-stable. The complexes can also tolerate the ester and ether functional groups and can polymerize **3**(3) to high molecular weight polymers with narrow molecular weight distributions, albeit in only moderate yields.

The polymerization behavior of **3**(4) is quite different from its counterparts with shorter spacer lengths. WCl_6 alone can already produce polymeric product in a moderate yield (~40%) at room temperature (Table 4, no. 1). Addition of Ph_4Sn leads to a decrease, instead of increase, in the polymer yield. Toluene is generally a poorer solvent than dioxane in the polymerizations of functional acetylene monomers,[19,20] but in this case, a high molecular weight polymer is obtained in a very

Table 4. Polymerization of 6-{[(4′-Heptoxy-4-biphenylyl)carbonyl]oxy}-1-hexyne [3(4)][a]

no.	catalyst	solvent	temp (°C)	yield (%)	M_w[b]	M_w/M_n[b]
1	WCl_6	dioxane	rt[c]	39.5	36200	2.81
2	WCl_6-Ph_4Sn	dioxane	rt	31.7	57600	2.62
3	WCl_6-Ph_4Sn	dioxane	60	87.3	112900	5.01
4	WCl_6-Ph_4Sn	toluene	rt	92.4	25400	1.89
5	WCl_6-Ph_4Sn	toluene	60	40.1	7240	1.28
6	$MoCl_5-Ph_4Sn$	dioxane	rt	19.4	34600	2.50

[a] Carried out under nitrogen for 24 h; $[M]_0$ = 0.2 M, [cat.] = ([cocat.] =) 10 mM. [b] Determined by GPC in THF on the basis of a polystyrene calibration. [c] rt = room temperature.

Table 5. Polymerization of 11-{[(4′-Heptoxy-4-biphenylyl)carbonyl]oxy}-1-undecyne} [3(9)][a]

no.	catalyst	solvent	temp (°C)	yield (%)	M_w[b]	M_w/M_n[b]
1	WCl_6	dioxane	rt[c]	26.2	51300	2.90
2	WCl_6-Ph_4Sn	dioxane	rt	41.7	63700	2.59
3	WCl_6-Ph_4Sn	dioxane	60	82.2	41200	2.21
4	WCl_6-Ph_4Sn	toluene	rt	58.4	13900	1.49
5	WCl_6-Ph_4Sn	toluene	60	51.2	6080	1.31
6	$MoCl_5-Ph_4Sn$	dioxane	rt	21.7	27000	2.21

[a] Carried out under nitrogen for 24 h; $[M]_0$ = 0.2 M, [cat.] = ([cocat.] =) 10 mM. [b] Determined by GPC in THF on the basis of a polystyrene calibration. [c] rt = room temperature.

Table 6. Polymerization of 5-{[(4′-Heptoxy-4-biphenylyl)oxy]carbonyl}-1-pentyne [4(3)][a]

no.	catalyst[b]	solvent	temp (°C)	yield (%)	M_w[c]	M_w/M_n[c]
1	WCl_6	dioxane	rt[d]	9.6	12700	1.55
2	WCl_6-Ph_4Sn	dioxane	rt	33.1	19200	2.04
3	WCl_6-Ph_4Sn	dioxane	60	64.3	19400	2.07
4	WCl_6-Ph_4Sn	toluene	rt	26.1	15300	1.69
5	WCl_6-Ph_4Sn	toluene	60	21.0	10600	1.44
6	$MoCl_5-Ph_4Sn$	dioxane	rt	19.2	12500	2.31
7	$W(mes)(CO)_3$	CCl_4	60	6.3	13500	1.77
8	$Mo(nbd)(CO)_4$	CCl_4	60	42.1	10400	1.60
9	$Fe(acac)_3-AlEt_3$	toluene	rt	35.4	5340	1.39

[a] Carried out under nitrogen for 24 h; $[M]_0$ = 0.2 M, [cat.] = ([cocat.] =) 10 mM; for Zielger-Natta catalyst, $[AlEt_3] = 3[Fe(acac)_3]$. [b] Abbreviations: mes = mesitylene, nbd = 2,5-norborndiene, acac = acetylacetonate. [c] Determined by GPC in THF on the basis of a polystyrene calibration. [d] rt = room temperature.

high yield (92.4%) when the polymerization of **3**(4) is carried out in toluene. In the polymerization of **3**(2) in toluene, increasing temperature leads to an increase in M_w (cf., Table 2, nos. 4 and 5). However, in the case of **3**(4), the opposite trend is observed, that is, M_w greatly drops as temperature increases (Table 4, nos. 4 and 5). Similar results are obtained in the polymerization of **3**(9) (Table 5, nos. 4 and 5), which also possesses a long spacer length. Thus, the monomers with longer alkyl spacers show polymerization behaviors in toluene distinctly different from those of the monomers with shorter spacers.

Similar to its cousin **3**(3), **4**(3) undergoes sluggish polymerization when WCl_6 alone is used as the catalyst in dioxane (Table 6, no. 1). Toluene is again a poor solvent for the polymerization of **4**(3), probably because it shares a common structural feature with **3**(3): both of them possess a short alkyl spacer. The results of the polymerizations of **4**(3) catalyzed by $MoCl_5-Ph_4Sn$ and $W(mes)(CO)_3$ are far from satisfactory, but the $Mo(nbd)(CO)_4$-initiated polymerization produces a polymer with

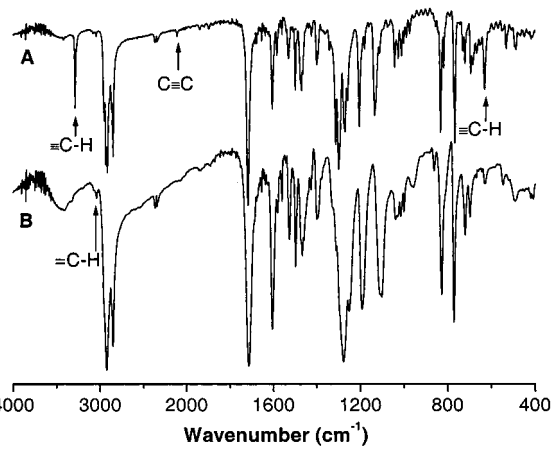

Figure 3. IR spectra of (A) **3**(9) and (B) its polymer **1**(9) (sample from Table 5, no. 3).

an M_w of ~10 000 in a good yield (Table 6, no. 8). In general, however, the polymerization results of **4**(3) are poorer than those of **3**(3) under the comparable experimental conditions. Akagi and Shirakawa have polymerized their mesogenic acetylene monomers with an ether functionality to high molecular weight polymers (M_w up to 3×10^6) in high yields (>65%) using $Fe(acac)_3-AlEt_3$ as catalyst.[15b] We have, however, found that $Fe(acac)_3-AlEt_3$ is a poor catalyst for the polymerization of **4**(3): it only gives an oligomeric product. This is probably due to the incompatible nature of the ester functionality with the Ziegler−Natta catalyst.

Structural Characterization. All the purified polymerization products give satisfactory spectroscopic data corresponding to their expected molecular structures. An example of the IR spectrum of **1**(9) is shown in Figure 3; for comparison, the spectrum of its monomer **3**(9) is also given. The monomer absorbs at 2114, 3286, and 630 cm^{-1}, due respectively to the C≡C stretching and ≡C−H stretching and bending vibrations. All these acetylene absorption bands disappear in the spectrum of its polymer, but the double-bond absorption at 3040 cm^{-1} intensifies (Figure 3B), indicating that the acetylene triple bonds have been transformed to the polyene double bonds by the polymerization reaction.

The NMR analysis offers more detailed information on the molecular structure of the polymer. As shown in Figure 4B, in the ^1H NMR spectrum of **1**(9), there is no peak in the absorption region of the acetylene protons (δ ~2.0). Instead, a new broad weak peak appears in the olefin absorption region (δ 6.4−5.5). It has been reported by Masuda and Higashimura that the cis olefin protons of a poly(1-alkyne), poly(3,3-dimethyl-1-pentyne), absorbs at δ 6.05.[31] In our previous study,[19c] we have found that the cis protons in a group of mesogen-containing poly(1-alkynes) (**6**) absorb in the chemical shift region of 6.26−5.88 and have proposed the following equation for the calculation of cis contents of the polymers

$$\text{cis content (\%)} = [A_{cis}/(A_{total}/9)] \times 100 \qquad (1)$$

where A_{cis} and A_{total} are respectively the integrated peak areas of the absorption by the cis olefin proton and of the *total* absorption by the aromatic and olefinic protons. Structurally **1**(9) is analogous to **6**. The absorption of **1**(9) peaking at δ 5.8 thus should be from its cis protons, and using eq 1, the cis content of **1**(9) is estimated to be

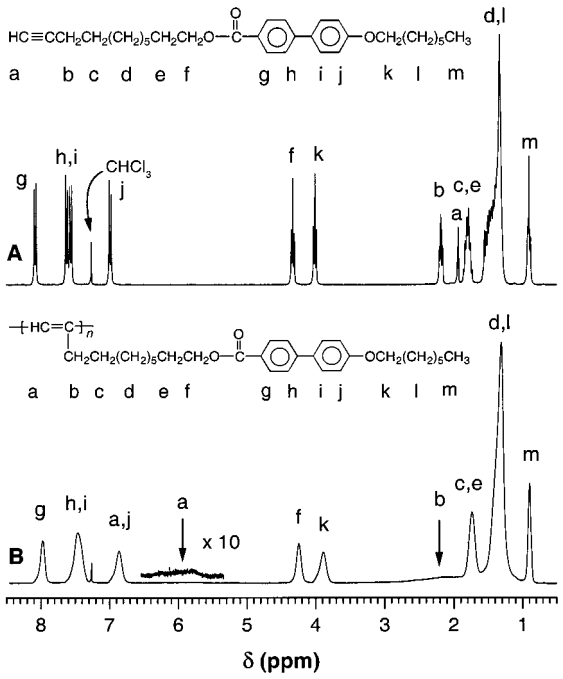

Figure 4. ^1H NMR spectra of (A) **3**(9) and (B) its polymer **1**(9) (Table 5, no. 3).

14.8% (or 85.2% trans). The polymer thus consists of predominantly trans structures and possesses a good stereoregularity, as reflected by its relatively sharp absorption peaks.[19c,32] From the comparison with the spectrum of its monomer, the broad absorption with a maximum at δ ~2.2 can be readily assigned to the absorption of the allylic proton adjacent to the polymer backbone ($CH_2C{=}C$). It is well-known that such structure can easily lose one hydrogen to from a stable allylic radical,[33] which may explain why the allylic absorption "peak" is so broad.

Figure 5 shows the ^{13}C NMR spectrum of **1**(9) along with that of its monomer **3**(9). While the acetylene carbon atoms of **3**(9) absorb at δ 84.7 and 68.1, these peaks disappear in the spectrum of **1**(9). The absorption peak of the propargyl carbon ($CH_2C{\equiv}C$) of **3**(9) at δ 18.4 also disappears because of its transformation to the allylic structure ($CH_2C{=}C$) in **1**(9) by the acetylene polymerization (noticing that a propargyl carbon absorbs at δ ~20 whereas an allylic carbon absorbs downfield at δ ~32[34]). The absorption peaks of the olefin carbon atoms of the polyacetylene backbone can, however, not be identified because of their overlapping with the peaks of the carbon atoms of the aromatic pendants.

The electronic absorption spectra of THF solutions of the polymers are given in Figure 6. Whereas none of the monomers absorbs photons with wavelengths longer than 325 nm, the polymers show absorption spectra extending into the visible spectral region, albeit with low molar absorptivity. The absorption in the long wavelength region is thus obviously from the double-bond backbones of the polyacetylenes. The low absorptivity suggests that the steric effect of the pendant groups have twisted the double bonds, reducing the effective conjugation lengths along the polyacetylene backbones. The absorption peaks of the alkoxybiphenylylcarbonyloxy pendants of **1**(*m*) are at ~296 nm, which is ~50 nm red-shifted from that of the biphenyl parent (246 nm).[34] The absorption of the heptoxybiphenylyloxycarbonyl chromophore of **2**(3) is however located

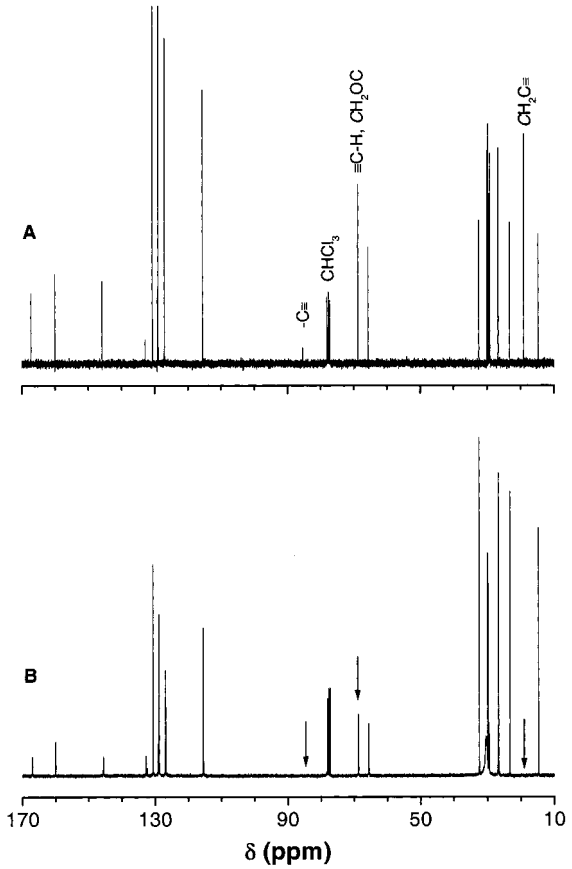

Figure 5. ^{13}C NMR spectra of (A) **3**(9) and (B) its polymer **1**(9) (Table 5, no. 3).

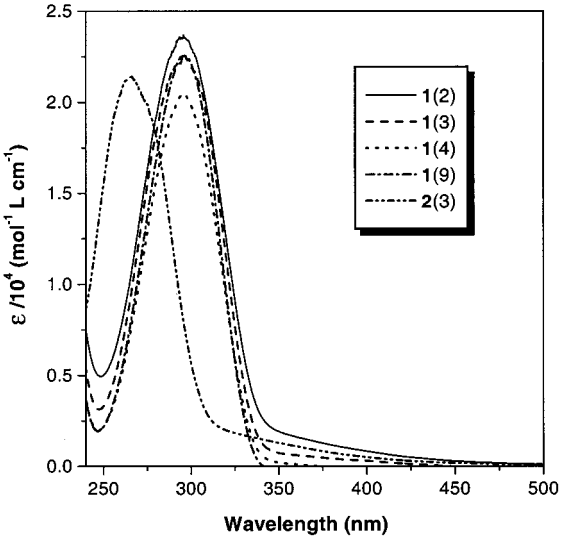

Figure 6. UV spectra of THF solutions of **1**(2) (sample from Table 2, no. 3), **1**(3) (Table 3, no. 4), **1**(4) (Table 4, no. 3), **1**(9) (Table 5, no. 3), and **2**(3) (Table 6, no. 3).

at 265 nm, which is more than 30 nm blue-shifted from that of its biphenylyl counterpart in **1**(3). This can be understood by the structural difference of the two mesogenic chromophores. The biphenylyl chromophore of **1**(3) is well polarized by the push−pull interaction of the electron-donating heptoxy and the electron-accepting carbonyloxy groups.[34,35] On the other hand, in **2**(3), both the heptoxy and oxycarbonyl groups are electron donating,[35] which still polarizes the biphenylyl chromophore but to a much lesser extent.

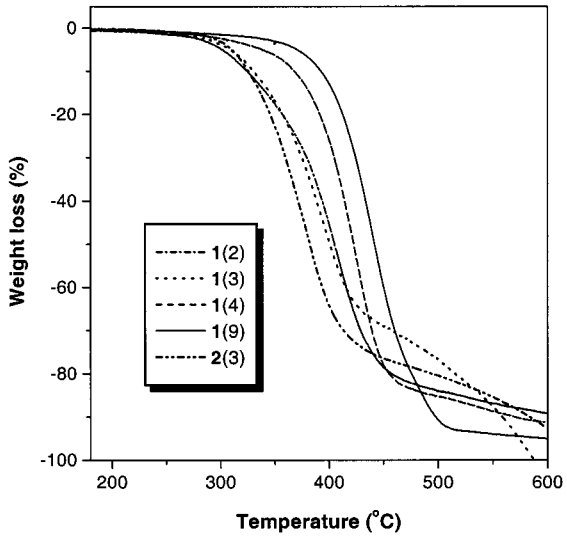

Figure 7. TGA thermograms of the mesomorphic polyalkynes **1**(2) (sample from Table 2, no. 3), **1**(3) (Table 3, no. 4), **1**(4) (Table 4, no. 3), **1**(9) (Table 5, no. 3), and **2**(3) (Table 6, no. 3) recorded under nitrogen at a heating rate of 10 °C/min.

Thermal and Mesomorphic Properties. Poly(1-alkynes) containing no mesogenic pendants such as poly(1-butyne) and poly(1-hexyne) {−[HC═C-(C_mH_{2m+1})]$_n$−, m = 2, 4} are very unstable and cannot even be isolated at room temperature from their polymerization mixtures without degradation.[36] As shown in Figure 7 **1**(m) and **2**(3) start to lose weight at high temperatures (≥300 °C) in the thermogravimetric analysis (TGA). Clearly, the introduction of the mesogenic groups as side chains into the poly(1-alkyne) structures has dramatically enhanced the thermal stability of the polymers.

Close inspection of the TGA thermograms reveals that the decomposition temperature (T_d) increases with the increase in the spacer length (m). The polymers may have not decomposed via an ester bond breakage mechanism because such a degradation route would give about the same T_d values for all the polymers. The decomposition of the polymers is probably by the pyrolytic cleavage of the allylic bond, cutting off the linkage between the mesogenic pendants (with different methylene units) and the polyacetylene backbones. Another possibility is via the backbiting cyclization route, as recently experimentally verified by us for the degradation of **5**.[20a] The resultant aromatization products of trisubstituted benzenes also possess different alkyl lengths and thus would evaporate at progressively higher temperatures.

After confirming the thermal stability of the polymers, we investigated their mesomorphic properties. Figure 8 shows the DSC thermograms of **1**(m) under nitrogen during the first cooling and the second heating scans. The thermogram recorded in the first cooling scan of **1**(2) displays a broad exothermic peak associated with the i−SmA transition at 170.7 °C, and the corresponding SmA−i transition is detected at 190.0 °C in the second heating scan. While the cooling curve provides no information on the T_g of the polymer, the endothermic baseline shift in the heating curve indicates that its glass transition occurs at ∼88.0 °C.

When the spacer length is increased to 3, the mesophasic transition peaks become sharper and the glass transition becomes readily detectable in both cooling and heating scans. This trend becomes more apparent

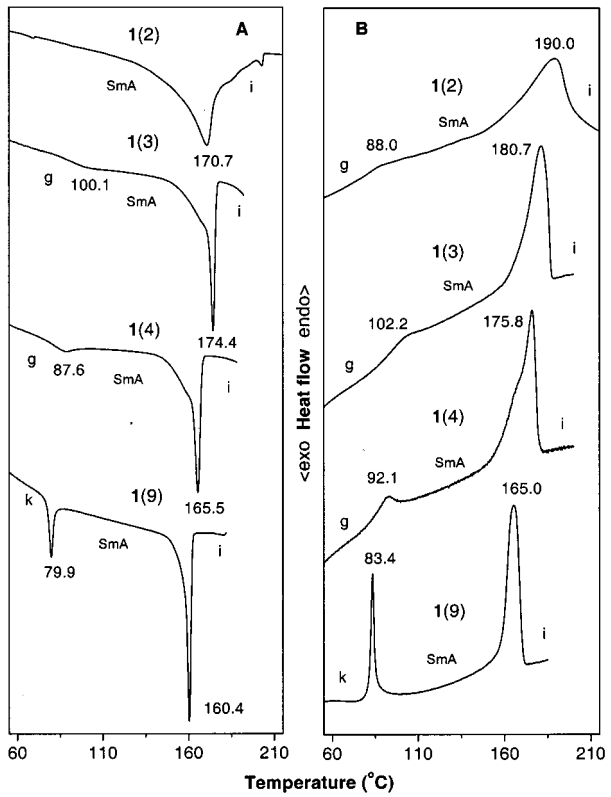

Figure 8. DSC thermograms of the mesomorphic polyacetylenes **1**(2) (sample from Table 2, no. 3), **1**(3) (Table 3, no. 4), **1**(4) (Table 4, no. 3), and **1**(9) (Table 5, no. 3) recorded under nitrogen during the (A) first cooling and (B) second heating scans at a scan rate of 10 °C/min.

when the spacer length is further increased to 4. Clearly, the longer spacer offers more freedom for the polymer segments and the mesogenic pendants to act separately. When the spacer length is increased to 9, the SmA ↔ i transition peaks become very sharp, and what is more, the peaks associated with melting/crystallization (k ↔ SmA) transitions can now be readily detected by the DSC analysis. This suggests that the polyacetylene backbones and the heptoxybiphenylylcarbonyloxy mesogens are well "decoupled" and that the mesogenic pendants can undergo the thermal transitions in a relatively independent fashion.

The mesogenic side chains are, however, not completely decoupled from the polymer main chains, as argued by other scientists.[37] Although the T_i of **1**(9) (165.0 °C) is the lowest among those of **1**(*m*), it is still much higher than that of its monomer **3**(9) (69.8 °C; cf. Table 1, no. 4). Apparently, the "polymer effect" is functioning. The macromolecular chains string the mesogenic pendants together in a comblike fashion, making the mesogens easy to order but difficult to randomize. The T_m of **1**(9) (83.4 °C) is also higher than that of **3**(9) (65.3 °C). The alkyl spacer in **3**(9) can melt at a relatively low temperature, and the thus-generated liquid will partially "dissolve" the crystalline structure of the monomer, bringing it into the liquid crystalline state. The movements of the alkyl spacers in **1**(9) are, however, restricted by the rigid polyacetylene backbones, and more energy or higher temperature is thus needed for the liquidation of the spacers and the partial dissolution of the crystalline structure of the mesogens. The higher transition temperatures of the polymers may also be explained by the virtual trimer model,[12,40] when two neighboring monomer repeat units (or a butadiene segment) in the polyacetylene backbone are considered. The "trimer" consists of three rigid cores, that is, two biphenyl and one butadiene moieties, whose large shape anisotropy would shift the thermal transitions to higher temperatures.

Figure 9 shows the POM microphotographs of the mesomorphic textures of **1**(*m*) and **2**(3). When **1**(2) is cooled from its isotropic state, small optically anisotropic entities emerge from the dark background of the isotropic liquid. The fine textures cannot grow to large monodomains, possibly because the mesogenic pendants are closely "coupled" with the rigid polyacetylene backbones, which partially distorts the packing arrangements of the mesogens and impedes the growth of the liquid crystalline domains. With the aid of X-ray diffraction (XRD) measurement, the textures are identified to be associated with a mixture of SmA phases (vide post).

When the spacer length is increased to 3, the anisotropic entities grow bigger (Figure 9B) but their development into typical focal-conic fan textures of SmA phase is still a somewhat difficult undertaking. The fan textures readily form when $m \geq 4$, thanks to the flexibility of the alkyl spacer, which allows the mesogens to move together to pack in a regular fashion. The polymer **2**(3) with a different ester orientation shows focal-conic fan textures (Figure 9D), which are obviously better developed than that of its structural cousin with the same length of alkyl spacer **1**(3). Thus, like in the case of their monomers, the orientation of the ester bridge also affects the mesophase formation of the polymers.

The thermal transitions and the corresponding enthalpy and entropy changes of the liquid crystalline polyacetylenes are summarized in Table 7. T_i and T_g generally decrease, though not to a great extent, with an increase in the spacer length *m*. Internal plasticization by the alkyl spacers may have played a role in decreasing the transition temperatures. It has been reported that poly(4-biphenyl acrylate), $-[CH_2-CH(CO_2\text{-Biph})]_n-$, shows smecticity while its closely related counterpart with a different orientation of ester bridge poly(vinyl 4-biphenylcarboxylate), $-[CH_2-CH(OCO\text{Biph})]_n-$, shows no mesomorphism.[39] The CO_2 (carbonyloxy) bridge allows better ordering, which is also found to be the case in our system. The polyacetylene with the CO_2 bridge [**2**(3)] shows higher T_i and T_g than the one with the OCO (oxycarbonyl) bridge [**1**(3)] ($\Delta T \sim 40$ °C; Table 7, nos. 4 and 2), in agreement with the POM observation that **2**(3) displays better developed mesomorphic textures. The monomer **4**(3) possesses a higher order of mesomorphism than **3**(3), and this superiority has been preserved even after **4**(3) has been polymerized.

Because of the better ordering packing in the SmA phase, the ΔH_i and ΔS_i involved in the SmA−i transitions are higher than those in the n−i transitions.[1,37] The large enthalpy and entropy changes involved in the mesophasic transitions of **1**(*m*) and **2**(3) rule out the possibility of nematicity and further support the assignment of smecticity to the mesophases of the polyacetylene liquid crystals. The ΔS value decreases in an alternative manner when *m* varies, with the even member exhibiting a larger value than does the odd one. Such results may again be explained by the virtual trimer model,[12,40] because trimeric mesogens have also

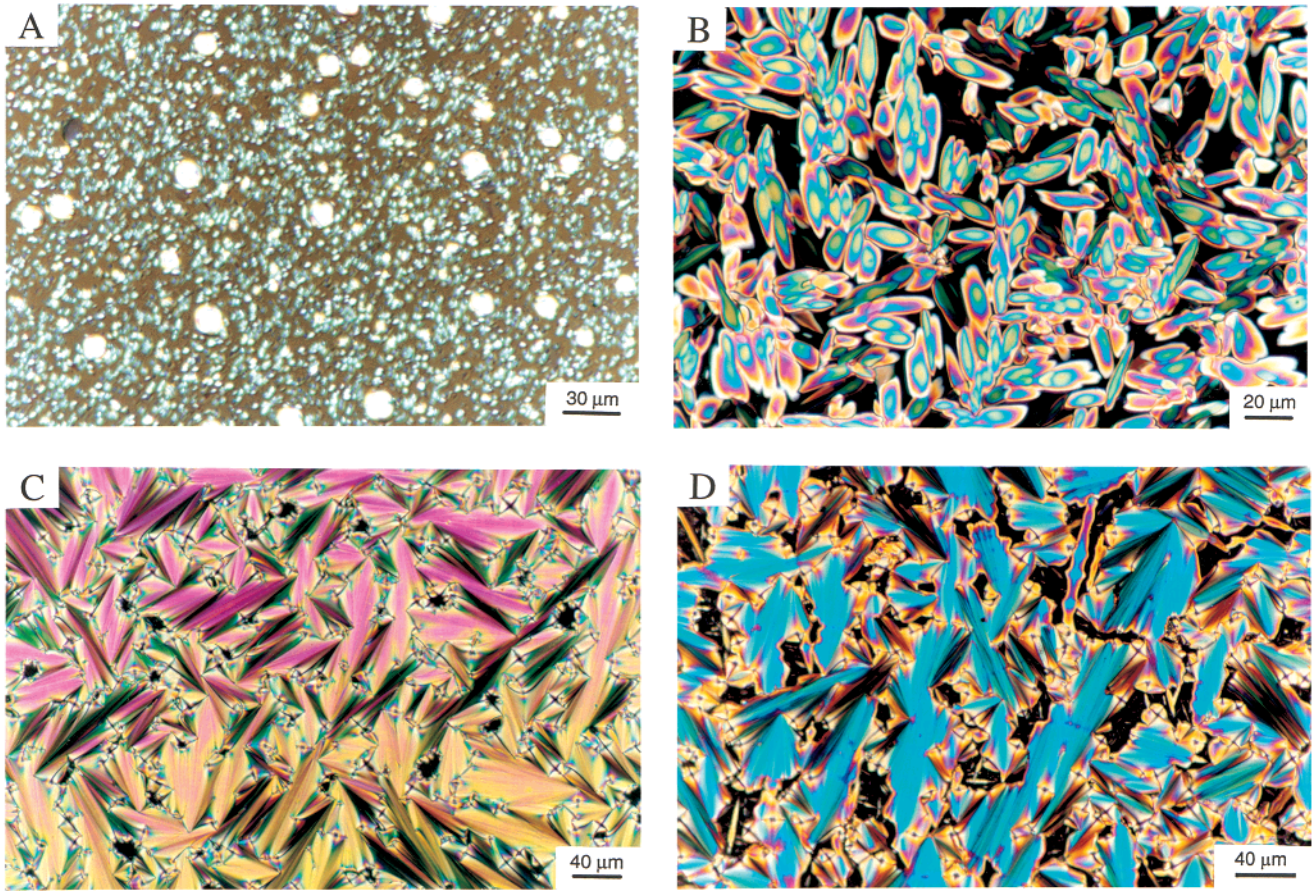

Figure 9. Mesomorphic textures observed on cooling (A) **1**(2) to 185.5 °C (sample from Table 2, no. 3), (B) **1**(3) to 175.0 °C (Table 3, no. 4), (C) **1**(9) to 145.0 °C (Table 5, no. 3), and (D) **2**(3) to 191.0 °C (Table 6, no. 3) from their isotropic states at a cooling rate of 1 °C/min.

Table 7. Thermal Transitions and Corresponding Thermodynamic Parameters of 1(*m*) and 2(3)[a]

		T, °C [Δ*H*, kJ/mru; Δ*S*, J/(mru K)][b]	
no.	polymer	cooling	heating
1	**1**(2)	i 170.7 (−8.97; −20.21) SmA	g 88.0 (−) SmA 190.0 (9.14; 19.73) i
2	**1**(3)	i 174.4 (−5.61; −12.53) SmA 100.1 (−) g	g 102.2 (−) SmA 180.7 (5.48; 12.07) i
3	**1**(4)	i 165.5 (−7.18; −16.37) SmA 87.6 (−) g	g 92.1 (−) SmA 175.8 (7.14; 15.90) i
4	**1**(9)	i 160.4 (−5.73; −13.22) SmA 79.9 (−1.13; −3.2) k	k 83.4 (1.42; 11.55) SmA 165.0 (6.25; 14.26) i
5	**2**(3)	i 205.5 (−4.95; −10.34) SmA 127.2 (−1.91; −4.77) g	g 140.9 (1.92; 4.64) SmA 218.1 (5.08; 10.34) i

[a] Data taken from the DSC thermograms recorded under dry nitrogen in the first cooling and second heating scans; abbreviations: k = crystalline state, Sm = smectic phase, g = glassy state, i = isotropic liquid. [b] Abbreviation: mru = monomer repeat unit.

Table 8. X-ray Diffraction Analysis Data of 1(*m*) and 2(3)[a]

polymer	*T* (°C)	d_1 (Å)	d_2 (Å)	d_3 (Å)	molecular length (*l*, Å)[b]	ratio d_1/l	phase
1(2)	181	32.94	22.64	4.39	22.67	1.45	SmA + SmA_d
1(3)	164	31.53	22.35	4.41	23.92	1.32	SmA + SmA_d
1(4)	153	25.22		4.39	25.16	1.00	SmA
1(9)	151	32.69	16.60	4.33	31.38	1.04	SmA
2(3)	185	41.25	21.85	4.42	23.35	1.77	SmA_d

[a] The mesophases in the liquid crystal states at the given temperatures were frozen by the rapid quenching with liquid nitrogen. [b] Calculated from the monomer repeat units in their fully extended conformation.

been found to show large entropy changes and similar odd−even effects.[41]

XRD analysis can provide useful information concerning molecular arrangement, mode of packing, and type of order in a mesophase of a polymeric liquid crystal. The XRD diffractogram of a powdery sample can be generally divided into the low-angle Bragg reflections at $2\theta \sim 3°$ corresponding to the layer spacing of molecular orientational order and the high-angle peaks at $2\theta \sim 20°$ associated with the two-dimensional liquidlike intermesogenic organization within the layers.[42] The appearance of a broad or sharp peak furnishes a qualitative indication of the degree of order.

The polymer with a spacer length of 2 shows an XRD pattern consisting of two low-angle peaks and one high-angle peak (Figure 10). The diffuse peak centered at $2\theta \sim 20°$ gives the average distance of the shorter preferred spacing (d_3 = 4.39 Å) occurring in the lateral packing arrangement of the mesogenic pendants (Table 8). The layer spacing derived from the Bragg reflection at $2\theta = 2.8°$ (d_1 = 32.94 Å) is longer than the molecular length (l = 22.67 Å) of one monomer repeat unit (mru) of **1**(2)

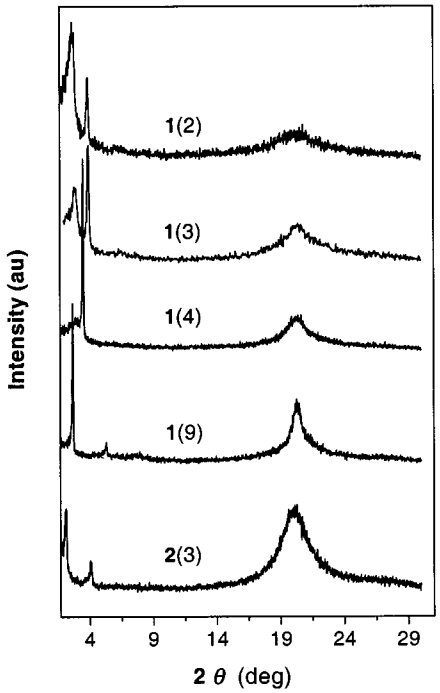

Figure 10. X-ray diffraction patterns of the mesomorphic polyalkynes quenched from their liquid crystalline states: (A) **1**(2) at 181 °C (sample from Table 2, no. 3), (B) **1**(3) at 164 °C (Table 3, no. 4), (C) **1**(4) at 153 °C (Table 4, no. 3), (D) **1**(9) at 151 °C (Table 5, no. 3), and (E) **2**(3) (Table 6, no. 3) at 185 °C.

at its most extended conformation, while that from the second peak at $2\theta = 3.95°$ ($d_2 = 22.64$ Å) corresponds well to one mru length within experimental error. The mesophase of **1**(2) thus involves both mono- and bilayer packing arrangements. Because the d_1/l ratio is ~1.5, the bilayer structure is thus an SmA_d type, in which the alkoxy tails are interdigitated in an antiparallel fashion. The mesogenic pendants in the SmA_d structure are, however, not well packed, as evidenced by the width of the first reflection peak at the lowest angle. The imperfect SmA_d packing and the mixture nature of the smectic phase (SmA + SmA_d) may be partially responsible for the broadness of its transition peaks (cf., Figure 8) and for the difficulty in growing the anisotropic entities into large-size monodomain textures (cf., Figure 9A).

Similarly, **1**(3) exhibits two high-angle Bragg reflections, from which the *d* spacings corresponding to the normal monolayer (SmA) and interdigitated bilayer (SmA_d) structures can be derived. Thus, the mesophase of **1**(3) also involves the mixed smectic packing arrangements. However, different from **1**(2), in this case, the sharp peak responsible for the monolayer structure is stronger in intensity than the broad one for the bilayer structure, indicating that the longer spacer promotes the monolayer arrangements, in which the mesogenic pendants are better packed.

When the spacer length is increased by one more methylene unit to 4, the reflection peak on the most left side of the diffractogram weakens in intensity to such an extent that its maximum cannot be easily identified. On the other hand, the Bragg reflection associated with the monolayer structure becomes very strong. In other words, the monolayer structure grows at the expense of the bilayer one. The further increment in the spacer length completely eliminates the SmA_d-related signals, and all the mesogens of **1**(9) are now packed in the monolayer structure (Chart 3A). Indeed, the packing is

Chart 3

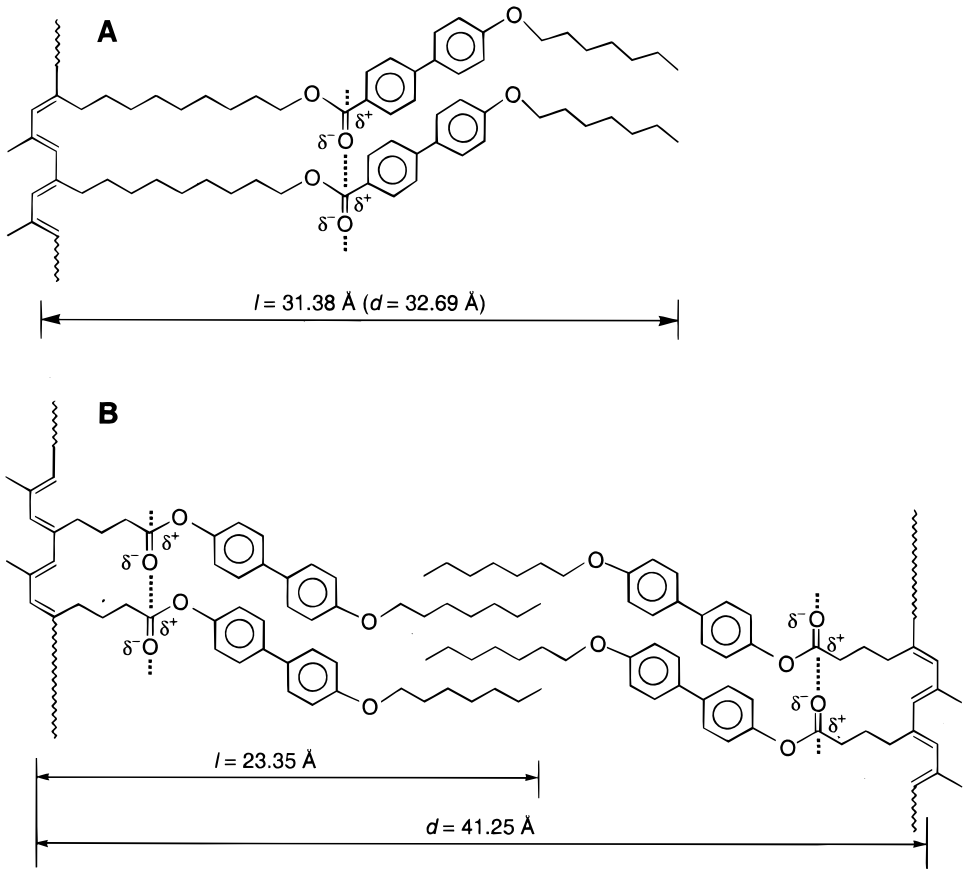

so regular that its higher-order secondary reflection at a middle angle of $2\theta = 5.32°$ ($d_2 = 16.60$ Å) can be readily detected by the XRD diffratometer.

The XRD diffratogram of **2**(3) also displays Bragg reflections at low and middle angles. The sharp reflection at the low angle of $2\theta = 2.1°$ corresponds to a layer spacing of $d_1 = 41.25$ Å, which is in considerable excess of the molecular length ($d_1/l = 1.77$). The mesogenic pendants of **2**(3) are thus packed in an interdigitated bilayer structure (Chart 3B). The peak at the middle angle $2\theta = 4.04°$ ($d_2 = 21.85$ Å) is obviously associated with the secondary reflection of the lamellar structure. Whereas the packing arrangements of **1**(3) consist of mixed mono- and bilayer structures, in the mesophase of **2**(3), only the bilayer structure is involved in the smectic packing of the mesogenic pendants. Clearly, the orientation of the ester connecting bridge dramatically affects the layer structure of the liquid crystalline polyacetylenes.

Conclusions

In this work, we designed and synthesized a group of mesogenic acetylene monomers and polymers with different spacer lengths and bridge orientations and investigated the effects of the structural variations on the chemical and physical properties of the (macro)-molecules. Our findings can be summarized as follows:

(1) All the acetylene monomers **3**(m) and **4**(3) are liquid crystalline, whose T_m and T_i decrease with an increase in the spacer length. The monomer with the ester bridge of the CO_2 orientation shows a better ordered mesophase and higher transition temperatures than does its counterpart with the OCO orientation.

(2) For the mesogenic monomers with shorter spacers ($m \leq 3$), the best polymerization results are obtained in the polar solvent of dioxane, while for those with longer spacers ($m \geq 4$), the nonpolar toluene is a better solvent under comparable polymerization conditions. The orientation of the ester bridge also affects the polymerizability of the monomers: **3**(3) generally performs better than **4**(3).

(3) The spacer length exerts little influence on the electronic transitions of the polymers. The ester orientation, however, affects the polarizability of the biphenyl core, with the electronic absorption of **2**(3) being considerably blue-shifted from that of **1**(3).

(4) All the polymers are thermally stable and their degradation temperature increases with the increase in the spacer length, regardless of the orientation of the ester bridge.

(5) The T_g and T_i of the polymers decrease as the spacer length increases. The packing arrangements of the mesogenic pendants change with the spacer length: while the smectic phases of **1**(m) with $m \leq 3$ consist of a mixture of mono- and bilayer structures, those with $m \geq 4$ possess a better ordered homogeneous monolayer structure. The orientation of the ester bridge also changes the mesomorphic properties of the polymers: compared to **1**(3), **2**(3) displays better developed mesomorphic textures, exhibits higher transition temperatures, and is better ordered in a homogeneous bilayer structure.

Thus, the structural changes in the spacer length and the bridge orientation alter the mesomorphism and polymerizability of the monomers and the electronic absorption, thermal stability, and packing order of the polymers. The structure−property relationships gained in this study are anticipated to help guide structural design endeavor in the development of new functional polyacetylenes with desirable properties.

Experimental Section

Materials. Dioxane (Nacalai Tesque), THF (Lab-Scan), and toluene (BDH) were predried over 4 Å molecular sieves and distilled from sodium benzophenone ketyl immediately prior to use. Dichloromethane (Lab-Scan) was dried over the molecular sieves and distilled over calcium hydride. 3-Butyn-1-ol, 4-pentyn-1-ol, 5-hexyn-1-ol, 10-undecyn-1-ol, and 4-pentynoic acid were the products of Farchan Laboratory and were used as received. Except for molybdenum(V) chloride (Acros), all other reagents and solvents were purchased from Aldrich and used without further purification.

Instrumentation. The IR spectra were measured on a Perkin-Elmer 16 PC FT-IR spectrophotometer. The ^{1}H and ^{13}C NMR spectra were recorded on a Bruker ARX 300 NMR spectrometer using chloroform-*d* as solvent and tetramethylsilane ($\delta = 0$) or chloroform (7.26) as internal reference. The UV spectra were measured on a Milton Roy Spectronic 3000 Array spectrophotometer and the molar absorptivities (ϵ) of the polymers were calculated on the basis of their repeat units. The mass spectra were recorded on a Finnigan TSQ 7000 triple quadrupole mass spectrometer operating in a chemical ionization (CI) mode using methane as carrier gas. The elemental analyses were performed by M−H−W, USA. The molecular weights of the polymers were estimated by a Waters Associates GPC system. THF was used as eluent at a flow rate of 1.0 mL/min. A set of Waters monodisperse polystyrene standards covering a molecular weight range of 10^3−10^7 were used for the molecular weight calibration.

The thermal stability of the polymers was evaluated on a Perkin-Elmer TGA 7 under nitrogen at a heating rate of 10 °C /min. A Perkin-Elmer DSC 7 was used to measure the phase transition thermograms. An Olympus BX 60 POM equipped with a Linkam TMS 92 hot stage was used to observe the anisotropic optical textures. The XRD patterns were recorded on a Philips PW1830 powder diffractometer with a graphite monochromator using a 1.5406 Å Cu Kα wavelength at room temperature (scanning rate 0.05 deg/s; scan range 1−30°). The polymer samples for the XRD measurements were prepared by freezing the molecular arrangements in the liquid crystalline states by liquid nitrogen as previously reported.[19c,21a]

Monomer Synthesis. The alkyne monomers **3**(m) were synthesized by etherification of 4′-hydroxy-4-biphenylcarboxylic acid with 1-bromoheptane followed by esterification with *n*-alkyn-1-ol in the presence of DCC, TsOH, and DMAP (cf., Scheme 1). The monomer **4**(3) with a different ester orientation was prepared by etherification of 4,4′-biphenol with 1-bromoheptane followed by esterification with 5-hexynoic acid. Typical synthetic procedures are given below.

4′-Heptoxy-4-biphenylylcarboxylic acid (16). In a 1000 mL Erlenmeyer flask equipped with a condenser were dissolved 10 g (46.7 mmol) of 4′-hydroxy-4-biphenylcarboxylic acid and 8 g of KOH (93.5 mmol) in 500 mL of an ethanol/water mixture (6:1 by volume) under gentle heating and stirring. To the homogeneous solution were added 12 g (67 mmol) of 1-bromoheptane and a catalytic amount of potassium iodide, and the resultant mixture was refluxed for 30 h. The reaction mixture was then poured into 300 mL of water and acidified with 20 mL of 37% hydrochloric acid. The precipitate was collected by suction filtration. Recrystallization in glacial acetic acid and drying in a vacuum oven gave 9 g of **16** as white crystals (yield: 61.7%). IR (KBr), ν (cm^{-1}): 3200−2300 (br, COOH), 1684 (s, C═O). ^{1}H NMR (300 MHz, DMSO-d_6), δ (ppm): 12.95 (s, 1H, CO_2H), 8.09 (d, 2H, Ar−H ortho to CO_2H), 7.86 (d, 2H, Ar−H meta to CO_2H), 7.79 (d, 2H, Ar−H meta to OC_7H_{15}), 7.15 (d, 2H, Ar−H ortho to OC_7H_{15}), 4.11 (t, 2H, $ArOCH_2$), 1.83 (m, 2H, OCH_2CH_2), 1.48 [m, 8H, $(CH_2)_4$], 0.97 (t, 3H, CH_3). ^{13}C NMR (75 MHz, DMSO-d_6), δ (ppm): 167.4 (C═O), 159.2 (aromatic carbon linked with OC_7H_{15}), 144.2 (aromatic carbon para to CO_2H), 131.3 (aromatic carbon para to OC_7H_5), 130.2 (aromatic carbons ortho to CO_2H), 129.1

(aromatic carbon linked with CO_2H), 128.3 (aromatic carbons meta to OC_7H_5), 126.3 (aromatic carbons meta to CO_2H), 115.2 (aromatic carbons ortho to OC_7H_5), 67.8 (OCH_2), 31.5 ($CH_2C_2H_5$), 28.9 ($CH_2C_3H_7$), 28.7 (OCH_2CH_2), 25.7 [$O(CH_2)_2CH_2$], 22.3 (CH_2CH_3), 14.2 (CH_3).

4-{[(4′-Heptoxy-4-biphenylyl)carbonyl]oxy}-1-butyne [3(2)]. In a typical run, 4′-heptoxy-4-biphenylylcarboxylic acid (2.0 g, 6.4 mmol), 3-butyn-1-ol (0.6 g, 8.6 mmol), TsOH (0.3 g, 1.7 mmol), and DMAP (0.2 g, 1.6 mmol) were dissolved in 250 mL of dry dichloromethane in a 500 mL two-necked round-bottom flask under an atmosphere of nitrogen. The solution was cooled to 0−5 °C with an ice−water bath, to which 2.0 g of DCC (9.7 mmol) in 50 mL of dichloromethane was added under stirring via a dropping funnel. The reaction mixture was stirred overnight. After filtering out the formed insoluble urea, the filtrate was concentrated by a rotary evaporator. The product was purified by a silica gel column using chloroform as eluent followed by recrystallization from absolute ethanol.

Characterization Data. 3(2): White solid; yield 76.6%. IR (KBr), ν (cm^{-1}): 3316 (s, H−C≡), 1720 (vs, C═O), 632 (m, H−C≡ bending). ^{1}H NMR (300 MHz, $CDCl_3$), δ (ppm): 8.11 (d, 2H, Ar−H ortho to CO_2), 7.64 (d, 2H, Ar−H meta to CO_2), 7.57 (d, 2H, Ar−H meta to OC_7H_{15}), 7.01 (d, 2H, Ar−H ortho to OC_7H_{15}), 4.45 (t, 2H, CH_2OCO), 4.01 (t, 2H, OCH_2), 2.69 (td, 2H, ≡C−CH_2), 2.04 (t, 1H, HC≡), 1.81 (m, 2H, OCH_2CH_2), 1.52−1.32 [m, 8H, $(CH_2)_4$], 0.90 (t, 3H, CH_3). ^{13}C NMR (75 MHz, $CDCl_3$), δ (ppm): 166.3 (C═O), 159.5 (aromatic carbon linked with OC_7H_{15}), 145.5 (aromatic carbon para to CO_2), 132.1 (aromatic carbon para to OC_7H_{15}), 130.2 (aromatic carbons ortho to CO_2), 128.3 (aromatic carbons meta to OC_7H_{15}), 127.9 (aromatic carbon linked to CO_2), 126.4 (aromatic carbons meta to CO_2), 114.9 (aromatic carbons ortho to OC_7H_{15}), 80.1 (≡C), 70.0 (HC≡), 68.1 (OCH_2), 62.5 (CH_2-OCOAr), 31.8 ($CH_2C_2H_5$), 29.2 ($CH_2C_3H_7$), 29.0 (OCH_2CH_2), 26.0 [$O(CH_2)_2CH_2$)], 22.6 (CH_2CH_3), 19.1 (≡C−CH_2), 14.1 (CH_3). MS (CI): *m/e* 365.2 [$(M + 1)^+$, calcd 365.2]. Anal. Calcd for $C_{24}H_{28}O_3$: C, 79.08; H, 7.75. Found: C, 79.17; H, 7.89.

3(3): White solid; yield 64.6%. IR (KBr), ν (cm^{-1}): 3280 (s, HC≡), 1712 (vs, C═O), 632 (m, ≡C−H bending). ^{1}H NMR (300 MHz, $CDCl_3$), δ (ppm): 8.09 (d, 2H, Ar−H ortho to CO_2R), 7.63 (d, 2H, Ar−H meta to CO_2), 7.57 (d, 2H, Ar−H meta to OC_7H_{15}), 6.99 (d, 2H, Ar−H ortho to OC_7H_{15}), 4.45 (t, 2H, CH_2-OCO), 4.01 (t, 2H, OCH_2), 2.41 (td, 2H, ≡C−CH_2), 2.01 (m, 3H, HC≡ and ≡CCH_2CH_2), 1.81 (m, 2H, OCH_2CH_2), 1.50−1.32 [m, 8H, $(CH_2)_4$], 0.90 (t, 3H, CH_3). ^{13}C NMR (75 MHz, $CDCl_3$), δ (ppm): 166.5 (C═O), 159.4 (aromatic carbon linked with OC_7H_{15}), 145.3 (aromatic carbon para to CO_2), 132.1 (aromatic carbon para to OC_7H_{15}), 130.1 (aromatic carbons ortho to CO_2R), 128.3 (aromatic carbons meta to OC_7H_{15}), 128.2 (aromatic carbon linked with CO_2R), 126.4 (aromatic carbons meta to CO_2), 114.9 (aromatic carbons ortho to OC_7H_{15}), 83.1 (≡C), 69.0 (HC≡), 68.1 (OCH_2), 63.4 (CH_2OCO), 31.8 ($CH_2C_2H_5$), 29.2 ($CH_2C_3H_7$), 29.0(OCH_2CH_2), 27.7 (≡C−CH_2CH_2), 26.0 [$O(CH_2)_2CH_2$], 22.6 (CH_2CH_2), 15.4 (≡C−CH_2), 14.1 (CH_3). MS (CI): *m/e* 379.3 [$(M + 1)^+$, calcd 379.2]. Anal. Calcd for $C_{25}H_{30}O_3$: C, 79.32; H, 7.99. Found: C, 79.34; H, 7.84.

3(4): White solid; yield 57.8%. IR (KBr), ν (cm^{-1}): 3276 (s, HC≡), 1710 (vs, C═O), 633 (m, ≡C−H bending). ^{1}H NMR (300 MHz, $CDCl_3$), δ (ppm): 8.09 (d, 2H, Ar−H ortho to CO_2), 7.63 (d, 2H, Ar−H meta to CO_2), 7.57 (d, 2H, Ar−H meta to OC_7H_{15}), 7.00 (d, 2H, Ar−H ortho to OC_7H_{15}), 4.37 (t, 2H, CH_2-OCO), 4.01 (t, 2H, OCH_2), 2.30 (td, 2H, ≡C−CH_2), 1.99 (t, 1H, HC≡), 1.95−1.67 (m, 6H, ≡C−CH_2CH_2, OCH_2CH_2, and CH_2-CH_2CO_2), 1.50−1.32 [m, 8H, $(CH_2)_4$], 0.90 (t, 3H, CH_3). ^{13}C NMR (75 MHz, $CDCl_3$), δ (ppm): 166.5 (C═O), 159.4 (aromatic carbon linked with OC_7H_{15}), 145.3 (aromatic carbon para to CO_2R), 132.1 (aromatic carbon para to OC_7H_{15}), 130.0 (aromatic carbons ortho to CO_2), 128.3 (aromatic carbons meta to OC_7H_{15}), 128.2 (aromatic carbon linked with CO_2), 126.4 (aromatic carbons meta to CO_2), 114.9 (aromatic carbons ortho to OC_7H_{15}), 83.9 (≡C), 68.7 (HC≡), 68.1 (OCH_2), 64.3 (CH_2-OCO), 31.8 ($CH_2C_2H_5$), 29.2 ($CH_2C_3H_7$), 29.0 (OCH_2CH_2), 27.8 (≡C−CH_2CH_2), 26.0 [$O(CH_2)_2CH_2$], 25.1 (CH_2CH_2OCO), 22.6 (CH_2CH_3), 18.1 (≡C−CH_2), 14.1 (CH_3). MS (CI): *m/e* 393.2 [$(M + 1)^+$, calcd 393.2]. Anal. Calcd for $C_{26}H_{32}O_3$: C, 79.54; H, 8.22. Found: C, 80.62; H, 8.09.

3(9): White solid; yield 88.0%. IR (KBr), ν (cm^{-1}): 3286 (s, HC≡), 1710 (vs, C═O), 630 (m, H−C≡ bending). ^{1}H NMR (300 MHz, $CDCl_3$), δ (ppm): 8.09 (d, 2H, Ar−H ortho to CO_2), 7.63 (d, 2H, Ar−H meta to CO_2), 7.57 (d, 2H, Ar−H meta to OC_7H_{15}), 6.99 (d, 2H, Ar−H ortho to OC_7H_{15}), 4.33 (t, 2H, CH_2-OCO), 4.00 (t, 2H, OCH_2), 2.19 (td, 2H, ≡C−CH_2), 1.94 (t, 1H, HC≡), 1.79 (m, 4H, ≡CCH_2CH_2 and $CH_2CH_2CO_2$), 1.61−1.34 [m, 20H, $2(CH_2)_5$], 0.91 (t, 3H, CH_3). ^{13}C NMR (75 MHz, $CDCl_3$), δ (ppm): 166.6 (C═O), 159.4 (aromatic carbon linked with OC_7H_{15}), 145.1(aromatic carbon para to CO_2), 132.2 (aromatic carbon para to OC_7H_{15}), 130.0 (aromatic carbons ortho to CO_2), 128.5 (aromatic carbons meta to OC_7H_{15}), 128.3 (aromatic carbon linked with CO_2), 126.4 (aromatic carbons meta to CO_2), 114.9 (aromatic carbons ortho to OC_7H_{15}), 84.7 (≡C), 68.1 (≡C−H and OCH_2), 65.0 (CH_2OCO), 31.8 ($CH_2C_2H_5$), 29.2 ($CH_2C_3H_7$), 29.0 (OCH_2CH_2), 29.3, 29.1, 28.9, 28.7, 28.6, 28.4, 25.9 (alkyl carbons), 26.0 [$O(CH_2)_2CH_2$], 22.7 (CH_2CH_3), 18.4 (≡C−CH_2), 14.1 (CH_3). MS (CI): *m/e* 463.3 [$(M + 1)^+$, calcd 463.3].

4′-Hydroxy-4-biphenylyl heptyl ether (19). Into a 500 mL Erlenmeyer flask equipped with a condenser was added 2.4 g (13 mmol) of 4′,4-biphenol, 0.7 g (13 mmol) of KOH, and 200 mL of an acetone/DMSO mixture (10:1 by volume). Under gentle heating and stirring, 1.2 g (6.7 mmol) of 1-bromoheptane and a catalytic amount of potassium iodide were added to the solution. The reaction mixture was refluxed for 24 h, poured into 200 mL of water, and acidified with 15 mL of 37% hydrochloric acid. The solid was collected by suction filtration and purified by a silica gel column using chloroform and chloroform/acetone (10/1) as eluents. Recrystallization in an ethanol/water mixture (3:1 by volume) gave 1.4 g of **19** as white solid (yield: 73.4%). IR (KBr), ν (cm^{-1}): 3380 (br, OH), 1250 and 1046 (s, C−O−C). ^{1}H NMR (300 MHz, $CDCl_3$), δ (ppm): 7.43 (m, 4H, Ar−H ortho to Ph), 6.90 (m, 4H, Ar−H meta to Ph), 4.90 (s, 1H, OH), 3.99 (t, 2H, OCH_2), 1.80 (m, 2H, OCH_2CH_2), 1.47−1.26 [m, 8H, $(CH_2)_4$], 0.90 (t, 3H, CH_3). ^{13}C NMR (75 MHz, $CDCl_3$), δ (ppm): 159.3 (aromatic carbon linked with OC_7H_{15}), 154.5 (aromatic carbon linked with OH), 133.8 (aromatic carbon para to OH), 133.2 (aromatic carbon para to OC_7H_{15}), 127.9 (aromatic carbons meta to OH), 127.7 (aromatic carbons meta to OC_7H_{15}), 115.8 (aromatic carbons ortho to OH), 114.8 (aromatic carbons ortho to OC_7H_{15}), 68.1 (OCH_2), 31.8 ($CH_2C_2H_5$), 29.3 ($CH_2C_3H_7$), 29.1 (OCH_2CH_2), 26.0 [$(OCH_2)_2CH_2$], 22.6 (CH_2CH_3), 14.1 (CH_3).

5-{[(4′-Heptoxy-4-biphenylyl)oxy]carbonyl}-1-pentyne [4(3)]. In a 500 mL round-bottom flask were dissolved 4′-hydroxy-4-biphenylyl heptyl ether (4 g, 14.1 mmol), 5-hexynoic acid (1.7 g, 15.2 mmol), DCC (4.4 g, 21.3 mmol), TsOH (1.3 g, 7.6 mmol), and DMAP (0.9 g, 7.4 mmol) in 300 mL of CH_2Cl_2. After the solution was stirred for 24 h, the formed urea was filtered out and dichloromethan was removed by a rotary evaporator. The residue was purified by a silica gel column using $CHCl_3$ as eluent. After recrystallization in absolute ethanol, 4.8 g of **4**(3) was isolated as white solid (yield: 90.0%). IR (KBr), ν (cm^{-1}): 3294 (s, HC≡), 1742 (vs, C═O), 630 (m, ≡C−H bending). ^{1}H NMR (300 MHz, $CDCl_3$), δ (ppm): 7.52 (m, 4H, Ar−H meta to Ph), 7.14 (d, 2H, Ar−H ortho to CO_2), 6.95 (d, 2H, Ar−H ortho to OC_7H_{15}), 4.00 (t, 2H, OCH_2), 2.75 (t, 2H, CH_2CO_2), 2.37 (td, 2H, ≡C−CH_2), 2.02 (m, 3H, ≡C−H and ≡C−CH_2CH_2), 1.81 (OCH_2CH_2), 1.48−1.33 [m, 8H, $(CH_2)_4$], 0.94 (t, 3H, CH_3). ^{13}C NMR (75 MHz, $CDCl_3$), δ (ppm): 171.7 (C═O), 158.8 (aromatic carbon linked with OC_7H_{15}), 149.5 (aromatic carbon linked with CO_2), 138.7 (aromatic carbon para to CO_2), 132.7 (aromatic carbon para to OC_7H_{15}), 128.0 (aromatic carbons meta to CO_2), 127.6 (aromatic carbons meta to OC_7H_{15}), 121.7 (aromatic carbons ortho to CO_2), 114.8 (aromatic carbons ortho to OC_7H_{15}), 83.1 (≡C), 69.4 (HC≡), 68.1 (OCH_2), 32.9 (CH_2CO_2), 31.8 ($CH_2C_2H_5$), 29.3 ($CH_2C_3H_7$), 29.0 (OCH_2CH_2), 26.0 [$O(CH_2)_2CH_2$], 23.5 ($CH_2CH_2CO_2$), 22.6 (CH_2CH_3), 17.8 (≡C−CH_2), 14.0 (CH_3). MS (CI): *m/e* 379.3 [$(M + 1)^+$, calcd 379.2].

Polymerization. All the polymerization reactions and manipulations were carried out under nitrogen using either

an inert-atmosphere glovebox (Vacuum Atmosphere) or Schlenk techniques in a vacuum line system, except for the purification of the polymers, which was done in an open atmosphere. A typical experimental procedure for the polymerization of **3**(2) is given below.

Into a baked 20 mL Schlenk tube with a stopcock in the sidearm was added 291.2 mg (0.8 mmol) of **3**(2). The tube was evacuated under vacuum and then flushed with dry nitrogen three times through the sidearm. Freshly distilled dioxane (2 mL) was injected into the tube to dissolve the monomer. The catalyst solution was prepared in another tube by dissolving 15.9 mg of WCl_6 and 17.2 mg of Ph_4Sn in 2 mL of dioxane. The two tubes were aged at 60 °C in an oil bath for 15 min and the monomer solution was transferred to the catalyst solution using a hypodermic syringe. The reaction mixture was stirred at 60 °C under nitrogen for 24 h. The solution was then cooled to room temperature, diluted with 5 mL of THF, and added dropwise to 500 mL of acetone through a cotton filter under stirring. The precipitate was allowed to stand overnight and was then filtered with a gooch crucible. The polymer was washed with acetone and dried in a vacuum oven at room temperature to a constant weight.

Characterization Data. 1(2): Red powdery solid; yield 72.4%. M_w 40800, M_w/M_n 2.22 (GPC; Table 2, no. 3). IR (KBr), ν (cm^{-1}): 1716 (C═O). ^1H NMR (300 MHz, $CDCl_3$), δ (ppm): 7.81, 7.21, 6.66 (Ar−H and trans ═C−H), 6.05 (cis ═C−H), 4.38 (CH_2OCO), 3.76 (OCH_2), 2.70 (═C−CH_2), 1.72 (OCH_2CH_2), 1.33 [$(CH_2)_4$], 0.96 (CH_3). ^{13}C NMR (75 MHz, $CDCl_3$), δ (ppm): 166.0 (C═O), 159.0 (aromatic carbon linked with OC_7H_{15}), 144.3 (aromatic carbon para to CO_2), 131.7 (aromatic carbon para to OC_7H_{15}), 130.0 (aromatic carbons ortho to CO_2), 128.0 (aromatic carbons meta to CO_2 and aromatic carbons linked with OC_7H_{15}), 126.0 (aromatic carbons meta to CO_2), 114.6 (aromatic carbons ortho to OC_7H_{15}), 67.9 ($ArOCH_2$), 62.5 (CH_2-OCO), 31.8 ($CH_2C_2H_5$ and ═C−CH_2), 29.3 ($CH_2C_3H_7$), 29.2 (OCH_2CH_2), 26.0 [$O(CH_2)_2CH_2$], 22.6 (CH_2CH_3), 14.1 (CH_3). UV (THF, 1.13×10^{-4} mol/L), $\lambda_{max}/\epsilon_{max}$: 296 nm/$2.37 \times 10^4$ mol^{-1} L cm^{-1}.

1(3): Orange powdery solid; yield 85.2%. M_w 49900, M_w/M_n 2.25 (GPC; Table 3, no. 4). IR (KBr), ν (cm^{-1}): 1714 (C═O). ^1H NMR (300 MHz, $CDCl_3$), δ (ppm): 7.83, 7.26, 6.70 (Ar−H and trans ═C−H), 6.00 (cis = C−H), 4.21 (CH_2OCO), 3.78 (OCH_2), 2.52 (═C−CH_2), 2.00(═C−CH_2CH_2), 1.69 (OCH_2CH_2), 1.29 [$(CH_2)_4$], 0.88 (CH_3). ^{13}C NMR (75 MHz, $CDCl_3$), δ (ppm): 166.1 (C═O), 159.1 (aromatic carbon linked with OC_7H_{15}), 144.5 (aromatic carbon para to CO_2), 132.5 (aromatic carbon para to OC_7H_{15}), 129.9 (aromatic carbons ortho to CO_2), 128.1 (aromatic carbons meta to CO_2 and aromatic carbons linked with OC_7H_{15}), 126.0 (aromatic carbons meta to CO_2), 114.6 (aromatic carbons ortho to OC_7H_{15}), 67.9 (OCH_2), 64.5 (CH_2-OCO), 31.8 ($CH_2C_2H_5$ and ═C−CH_2), 29.3 ($CH_2C_3H_7$), 29.1 (OCH_2CH_2), 26.0 [$O(CH_2)_2CH_2$], 22.6 (CH_2CH_3), 14.1 (CH_3). UV (THF, 1.2×10^{-4} mol/L), $\lambda_{max}/\epsilon_{max}$: 296 nm/$2.26 \times 10^4$ mol^{-1} L cm^{-1}.

1(4): Pale orange solid; yield 87.3%. M_w 112900, M_w/M_n 5.01 (GPC; Table 4, no. 3). IR (KBr), ν (cm^{-1}): 1714 (C═O). ^1H NMR (300 MHz, $CDCl_3$), δ (ppm): 7.87, 7.34, 6.91 (Ar−H and trans ═C−H), 5.94 (cis ═C−H), 4.20 (CH_2OCO), 3.79 (OCH_2), 2.18 (═C−CH_2 and ═C−CH_2CH_2), 1.75 (CH_2CH_2OCO), 1.29 [$(CH_2)_3$], 0.89 (CH_3). ^{13}C NMR (75 MHz, $CDCl_3$), δ (ppm): 166.1 (C═O), 159.1 (aromatic carbon linked with OC_7H_{15}), 144.5 (aromatic carbon para to CO_2), 131.8 (aromatic carbon para to OC_7H_{15}), 129.9 (aromatic carbons ortho to CO_2), 128.1 (aromatic carbons meta to CO_2 and aromatic carbons linked with OC_7H_{15}), 126.0 (aromatic carbons meta to CO_2), 114.6 (aromatic carbons ortho to OC_7H_{15}), 67.9 (OCH_2), 64.8 (CH_2-OCO), 31.8 ($CH_2C_2H_5$ and ═C−CH_2), 29.3 ($CH_2C_3H_7$), 29.1 (OCH_2CH_2), 26.0 [$O(CH_2)_2CH_2$], 22.6 (CH_2CH_3), 14.1 (CH_3). UV (THF, 1.1×10^{-4} mol/L), $\lambda_{max}/\epsilon_{max}$: 295 nm/$2.04 \times 10^4$ mol^{-1} L cm^{-1}.

1(9): Yellow powdery solid; yield 82.3%. M_w 41200, M_w/M_n 2.21 (GPC; Table 5, no. 3). IR (KBr), ν (cm^{-1}): 1714 (C═O). ^1H NMR (300 MHz, $CDCl_3$), δ (ppm): 7.97, 7.46, 6.86 (Ar−H and trans ═C−H), 5.80 (cis ═C−H), 4.25 (CH_2OCO), 3.89 (OCH_2), 2.18 (═C−CH_2), 1.74 (═CCH_2CH_2 and OCH_2CH_2), 1.31 [$2(CH_2)_5$], 0.90 (CH_3). ^{13}C NMR (75 MHz, $CDCl_3$), δ (ppm): 166.3 (C═O), 159.3 (aromatic carbon linked with OC_7H_{15}), 144.9 (aromatic carbon para to CO_2), 132.0 (aromatic carbon para to OC_7H_{15}), 130.0 (aromatic carbons ortho to CO_2), 128.5 (aromatic carbons meta to CO_2 and aromatic carbons linked with OC_7H_{15}), 128.1, 126.2 (aromatic carbons meta to CO_2), 114.8 (aromatic carbons ortho to OC_7H_{15}), 68.0 (CH_2-OCO), 64.9 (OCH_2), 31.8 ($CH_2C_2H_5$ and ═C−CH_2), 29.8, 29.7, 29.3 ($CH_2C_3H_7$), 29.1 (OCH_2CH_2), 28.8, 26.1, 26.0 [$O(CH_2)_2CH_2$], 22.6 (CH_2CH_3), 14.0 (CH_3). UV (THF, 9×10^{-5} mol/L), $\lambda_{max}/\epsilon_{max}$: 296 nm/$2.26 \times 10^4$ mol^{-1} L cm^{-1}.

2(3): Yellow powdery solid; yield 64.3%. M_w 19410, M_w/M_n 2.07 (GPC; Table 6, no. 3). IR (KBr), ν (cm^{-1}): 1756 (C═O). ^1H NMR (300 MHz, $CDCl_3$), δ (ppm): 7.26, 6.95, 6.78 (Ar−H and trans ═C−H), 6.10 (cis ═C−H), 3.86 (OCH_2), 2.56 (CH_2-CO_2 and ═C−CH_2), 1.77 (═C−CH_2CH_2 and $OCH_2CH_2CH_2$), 1.35 [$(CH_2)_4$], 0.93 (CH_3). ^{13}C NMR (75 MHz, $CDCl_3$), δ (ppm): 171.7 (C═O), 158.6 (aromatic carbon linked with OC_7H_{15}), 149.6 (aromatic carbon linked with OCOR), 138.0 (aromatic carbon para to CO_2), 132.2 (aromatic carbon para to OC_7H_{15}), 127.8 (aromatic carbons meta to CO_2), 127.3 (aromatic carbons meta to OC_7H_{15}), 121.8 (aromatic carbons ortho to CO_2), 114.6 (aromatic carbons ortho to OC_7H_{15}), 67.9 (OCH_2), 33.9 (CH_2-CO_2), 31.8 ($CH_2CH_2CH_3$), 29.4 ($CH_2C_3H_7$), 29.2 (OCH_2CH_2), 26.0 [$O(CH_2)_2CH_2$], 24.1 ($CH_2CH_2CO_2$), 22.6 (CH_2CH_3), 14.1 (CH_3). UV (THF, 1.38×10^{-4} mol/L), $\lambda_{max}/\epsilon_{max}$: 265 nm/$2.15 \times 10^4$ mol^{-1} L cm^{-1}.

Acknowledgment. The work described in this paper was partially supported by the grants of the Research Grants Council of the Hong Kong Special Administrative Region, China (Project Nos. HKUST597/95P, 6149/97P, and 6062/98P). This project was also benefited from the financial support of the Industry Department of the Hong Kong SAR Government. We thank Prof. Hoi Sing Kwok of the Department of Electrical and Electronic Engineering of our university and Prof. Zhishen Mo of the Laboratory of Polymer Physics of the Changchun Institute of Applied Chemistry for their helpful discussions.

References and Notes

(1) (a) Chigrinov, V. G. *Liquid Crystal Devices: Physics and Applications*; Artech House: Boston, MA, 1999. (b) *Liquid Crystals: Physics, Technology, and Applications*; Rutkowska, J., Ed.; SPIE-The International Society for Optical Engineering: Bellingham, WA, 1998. (c) *Handbook of Liquid Crystals*; Demus, D., Goodby, J., Gray, G. W., Spiess, H. W., Vill, V, Eds.; VCH: Weinheim, Germany, 1998. (d) *Handbook of Liquid Crystal Research*; Collings, P. J., Patel, J. S., Eds.; Oxford University Press: New York, 1997.

(2) (a) *Electrical and Optical Polymer Systems*; Wise, D. L., Wnek, G. E., Trantolo, D. J., Cooper, T. M., Gresser, J. D., Eds.; Marcel Dekker: New York, 1998. (b) *Photonic Polymer Systems*; Wise, D. L., Wnek, G. E., Trantolo, D. J., Cooper, T. M., Gresser, J. D., Eds.; Marcel Dekker: New York, 1998. (c) *Conjugated Polymers: the Novel Science and Technology of Highly Conducting and Nonlinear Optically Active Materials*; Bredas, J. L., Silbey, R., Eds.; Kluwer Academic: Boston, MA, 1991. (d) *Conjugated Polymeric Materials: Opportunities in Electronics, Optoelectronic and Molecular Electronic*; Bredas, J. L., Chance, R. R., Eds.; Kluwer Academic: Boston, MA, 1990.

(3) Katz, H. E. *J. Mater. Chem*. **1997**, *7*, 369.

(4) Burroughes, J. H.; Bradley, D. D. C.; Brown, A. R.; Marks, R, N.; Mackay, K.; Friend, R. H.; Burn, P. L.; Kraft, A.; Holmes, A. B. *Nature* **1990**, *347*, 539.

(5) Gustatsson, G.; Cao, Y.; Treacy, G. M.; Klavetter, F.; Colaneri, N.; Heeger, A. J. *Nature* **1992**, *357*, 477.

(6) Lüssem.; Festag, R.; Greiner, A.; Schmidt, C.; Unterlechner, C.; Heitz, W.; Wendorff, J. H.; Hopmeier, M.; Feldmann, J. *Adv. Mater*. **1995**, *7*, 923.

(7) Chen, S. H.; Conger, B. M.; Mastrangelo, J. C.; Kenda, A. S.; Kim, D. U. *Macromolecules* **1998**, *31*, 8051.

(8) Yoshino, K.; Yin, X. H.; Morita, S.; Nakazono, M.; Kawai, T.; Ozaki, M.; Jin, S. H.; Choi, S. K. *Jpn. J. Appl. Phys.* **1993**, *32*, L1673.
(9) Platé, N. A.; Shibaev, V. P. *Comb-Shaped Polymers and Liquid Crystals*; Plenum Press: New York, 1987.
(10) Cowie, J. M. G. *Polymers: Chemistry & Physics of Modern Materials*, 2nd ed.; Blackie Academic & Professional: London, 1991.
(11) Hsu, C. S. *Prog. Polym. Sci.* **1997**, *22*, 829. (b) Hsiech, C. J.; Wu, S. H.; Hsiue, G. H.; Hsu, C. S. *J. Polym. Sci., Polym. Chem. Ed.* **1994**, *32*, 1077.
(12) Imrie, C. T.; Schleeh, T.; Karasz, F. E.; Attard, G. S. *Macromolecules* **1993**, *26*, 539. (b) Imrie, C. T.; Luckhurst, G. R. In ref 1c; Chapter X, pp 801−833.
(13) *Polymer Handbook*, 4th ed.; Brandrup, J., Immergut, E. H., Grulke, E. A., Eds.; Wiley: New York, 1999.
(14) Masuda, T.; Tang, B. Z.; Tanaka, T.; Higashimura, T. *Macromolecules* **1986**, *19*, 1459.
(15) (a) Levon, K.; Park, K. C.; Pashkovski, E. In ref 2a; Chapter 5, pp 137−165. (b) Akagi, K.; Shirakawa, H. In ref 2a; Chapter 28, pp 983−1010. (c) Choi, S.-K.; Lee, J.-H.; Kang, S.-J.; Jin, S.-H. *Prog. Polym. Sci.* **1997**, *22*, 693.
(16) (a) Percec, V.; Asandei, A. D.; Hill, D. H.; Crawford, D. *Macromolecules* **1999**, *32*, 2597. (b) Chen, S. H.; Mastrangelo, J. C.; Conger, B. M.; Kende, A. D. *Macromolecules* **1998**, *31*, 3391. (c) Watanabe, Y.; Mihara, T.; Koide, N. *Macromol. Chem. Phys.* **1998**, *199*, 977. (d) Kijima, M.; Hasegawa, H.; Shirakawa, H. *J. Polym. Sci., Part A: Polym. Chem.* **1998**, *35*, 2691. (e) Gabaston, L, I.; Foot, P. J. S.; Brown, J. W. *Chem. Commun.* **1996**, 429. (f) Vincentini, F.; Barrceillet, J.; Laversanne, R.; Mauzac, M.; Bibonne, F.; Parneiz, J. P. *Liq. Cryst.* **1995**, *19*, 235. (g) Lieser, G.; Wegner, G. *Macromolecules* **1994**, *27*, 1027. (h) Thobie-Gauthier, C.; Bouligand, Y.; Gourges, A.; Jubault, M.; Roncali, J. *Adv. Mater.* **1994**, *6*, 138.
(17) (a) Yoshino, K.; Kobayashi, K.; Myofin, K, Ozaki, M.; Akagi, K.; Goto, H.; Shirakawa, H. *Jpn. J. Appl. Phys.* **1996**, *35*, 3964. (b) Shirakawa, H.; Kadokura, Y.; Goto, H.; Oh, S.-Y.; Akagi, K.; Araya, K. *Mol. Cryst. Liq. Cryst.* **1994**, *255*, 213. (c) Oh, S.-Y.; Akagi, K.; Shirakawa, H.; Araya, K. *Macromolecules* **1993**, *26*, 620.
(18) Koltzenburg, S.; Wolff, P.; Stelzer, F.; Springer, J.; Nuyken, O. *Macromolecules* **1998**, *31*, 9166.
(19) (a) Tang, B. Z.; Xu, K.; Sun, Q.; Lee, P. P. S.; Peng, H.; Salhi, F.; Dong, Y. In *Transition Metal Catalysis in Macromolecular Design*; Boffa, L. S.; Novak, B. M., Eds.; American Chemical Society: Washington, DC, 2000; Chapter 9, pp 146−164. (b) Tang, B. Z.; Kong, X.; Wan, X.; Feng, X.-D. *Macromolecules* **1998**, *31*, 7118. (c) Tang, B. Z.; Kong, X.; Wan, X.; Peng, H.; Lam, W. Y.; Feng, X.-D.; Kwok, H. S. *Macromolecules* **1998**, *31*, 2419. (d) Tang, B. Z.; Kong, X.; Wan, X.; Feng, X.-D. *Macromolecules* **1997**, *30*, 5620. (e) Tang, B. Z.; Poon, W. H.; Leung, S. M.; Leung, W. H.; Peng, H. *Macromolecules* **1997**, *30*, 2209.
(20) (a) Kong, X.; Lam, J. W. Y.; Tang, B. Z. *Macromolecules* **1999**, *32*, 1722. (b) Sun, Q.; Tang, B, Z. *Polym. Prepr.* **1999**, *40* (1), 558. (c) Cheuk, K. K. L.; Lam, J. W. Y.; Sun, Q.; Cha, J. A. K.; Tang, B. Z. *Polym. Prepr.* **1999**, *40* (2), 655. (d) Xu, H. Y.; Guang, S. Y.; Tang, B. Z. *Chin. Chem. Lett.* **2000**, *11*, 21. (e) Cheuk, K. K. L.; Lam, J. W. Y.; Cha, J. A. K.; Tang, B. Z. *Polym. Mater. Sci. Eng.* **2000**, *82*, 54. (f) Cheuk, K. K. L.; Lam, J. W. Y.; Tang, B. Z. *Polym. Mater. Sci. Eng.* **2000**, *82*, 56. (g) Cheuk, K. K. L.; Lam, J. W. Y.; Cha, J. A. K.; Tang, B. Z. *Polym. Prepr.* **2000**, *41* (1), 131.
(21) (a) Kong, X.; Tang, B. Z. *Chem. Mater.* **1998**, *10*, 3352. (b) Kong, X.; Wan, X.; Kwok, H. S.; Feng, X.-D.; Tang, B. Z. *Chin. J. Polym. Sci.* **1998**, *16*, 185. (c) Tang, B. Z.; Kong, X.; Feng, X.-D. *Chin. J. Polym. Sci.* **1999**, *17*, 289. (d) Huang, Y.; Bu, L.; Zhang, D.; Su, C.; Xu, Z.; Lam, J. W. Y.; Tang, B. Z. *J. Funct. Polym.* **1999**, *12*, 376. (e) Lam, J. W. Y.; Kong, X.; Kwok, H. S.; Tang, B. Z. *Polym. Mater. Sci. Eng.* **2000**, *82*, 91. (f) Lam, J. W. Y.; Cheuk, K. K. L.; Tang, B. Z. *Polym. Prepr.* **2000**, *41* (1), 912. (g) Lam, J. W. Y.; Cheuk, K. K. L.; Tang, B. Z. *Polym. Prepr.* **2000**, *41* (1), 969.
(22) (a) Huang, Y. M.; Lam, J. W. Y.; Cheuk, K. K. L.; Ge, W.; Tang, B. Z. *Macromolecules* **1999**, *32*, 5976. (b) Huang, Y. M.; Ge, W.; Lam, J. W. Y.; Tang, B. Z. *Appl. Phys. Lett.* **1999**, *307*, 67. (c) Lee, P. P. S.; Geng, Y. H.; Kwok, H. S.; Tang, B. Z. *Thin Solid Films* **2000**, *363*, 149. (d) Xu, H.; Sun, Q.; Lee, P. P. S.; Kwok, H. S.; Tang, B. Z. *Thin Solid Films* **2000**, *363*, 143. (e) Cheuk, K. K. L.; Lam, J. W. Y.; Sun, Q.; Cha, J. A. K.; Tang, B. Z. *Polym. Prepr.* **2000**, *41* (1), 981. (f) Lam, J. W. Y. M.Phil. Thesis, Hong Kong University of Science & Technology, Aug 1998.
(23) (a) Tang, B. Z.; Chen, H. Z.; Xu, R. S.; Lam, J. W. Y.; Cheuk, K. K. L.; Wong, H. N. C.; Wang, M. *Chem. Mater.* **2000**, *12*, 213. (b) Lee, C. W.; Wong, K. S.; Lam, W. Y.; Tang, B. Z. *Chem. Phys. Lett.* **1999**, *307*, 67. (c) Tang, B. Z.; Poon, W. H.; Peng, H.; Wong, H. N. C.; Ye, X.; Monde, T. *Chin. J. Polym. Sci.* **1999**, *17*, 81. (d) Huang, Y. M.; Lam, J. W. Y.; Cheuk, K. K. L.; Ge, W.; Tang, B. Z. *Macromolecules*, submitted for publication. (e) Tang, B. Z.; Lam. J. W. Y.; Kong, X.; Kwok, H. S. US Patent Appl. No. 09/352778, 1999.
(24) (a) Tang, B. Z.; Lam, J. W. Y.; Kong, X.; Lee, P. P. S.; Wan, X.; Kwok, H. S.; Huang, Y.; Ge, W.; Chen, H.; Xu, R.; Wang, M. In *Liquid Crystals III*; Khoo, I.-C., Ed.; SPIE-The International Society for Optical Engineering: Bellingham, WA, 1999; pp 62−71. (b) Wong, K. S.; Lee, C. W.; Tang, B. Z. *Synth. Met.* **1999**, *101*, 505. (c) Tang, B. Z.; Xu, H. *Macromolecules* **1999**, *32*, 2569. (d) Xu, H.; Tang, B. Z. *J. Macromol. Sci., Pure Appl. Chem.* **1999**, *A36*, 1197. (e) Huang, Y. M.; Lam, J. W. Y.; Cheuk, K. K. L.; Ge, W.; Tang, B. Z. *Thin Solid Films* **2000**, *363*, 146.
(25) (a) Gray, G. W.; Goodby, J. W. G. *Smectic Liquid Crystals: Texture and Structures*; Leonard Hill: London, 1984. (b) Demus, D.; Richter, L. *Textures of Liquid Crystals*; Verlag Chemie: Weinheim, Germany, 1978.
(26) Stevens, M. P. *Polymer Chemistry: an Introduction*, 3rd ed.; Oxford University Press: New York, 1999. (b) Johansson, G.; Percec, V.; Ungar, G.; Smith, K. *Chem. Mater.* **1997**, *9*, 164.
(27) Coates, D.; Gray, G. W. *Microscopy* **1976**, *24*, 117.
(28) Zhang, X.; Ozcayir, Y.; Feng, C.; Blumstein, A. *Polym. Prepr.* **1990**, *31*, 597.
(29) Gray, G. W. *Adv. Liq. Cryst.* **1976**, *2*, 1.
(30) (a) Masuda, T. In *Catalysis in Precision Polymerization*; Kobayashi, S., Ed.; Wiley: New York, 1997; pp 67−97. (b) Shirakawa, H.; Masuda, T.; Takeda, K. In *The Chemistry of Triple-Bonded Functional Groups*; Patai, S., Ed.; Wiley: New York, 1994; Supplement C2; Vol. 2; Chapter 17, pp 945−1016. (c) Wallace, K. C.; Liu, A. H.; Dewan, J. C.; Schrock, R. R. *Organometallics* **1989**, *8*, 644. (d) Grubbs, R. H.; Tumas, W. *Science* **1989**, *243*. 907. (e) Simionescu, C. I.; Percec, V. *Prog. Polym. Sci.* **1982**, *8*, 133.
(31) Okano, Y.; Masuda, T.; Higashimura, T. *J. Polym. Sci., Polym. Chem. Ed.* **1985**, *23*, 2637.
(32) Tonelli, A. P. *NMR Spectroscopy and Polymer Microstructure*; VCH: New York, 1989.
(33) (a) Barton, H. R. *Half a Century of Free Radical Chemistry*; Cambridge University Press: New York, 1993. (b) Moad, G.; Solomon, D. H. *The Chemistry of Free Radical Polymerization*; Pergamon: Tarrytown, NY, 1995.
(34) Silverstein, R. M.; Bassler, G. C.; Morrill, T. C. *Spectrometric Identification of Organic Compounds*, 5th ed.; Wiley: New York, 1991.
(35) Walter, W. *Beyer-Walter Handbook of Organic Chemistry*; Prentice Hall: London, 1996. (b) March, J. *Advanced Organic Chemistry*, 4th ed.; Wiley: New York, 1992.
(36) (a) Masuda, T.; Okano, Y.; Tamura, K.; Higashimura, T. *Polymer* **1985**, *26*, 793. (b) Masuda, T.; Tang, B. Z.; Higashimura, T.; Yamaoka, H. *Macromolecules* **1985**, *18*, 2369.
(37) (a) Pugh, C.; Kiste, A. L. *Prog. Polym. Sci.* **1997**, *22*, 601. (b) Percec, V.; Pugh, C. In *Side Chain Liquid Crystalline Polymers*; McArdle, C. B., Ed.; Chapman & Hall: New York, 1989; Chapter 3, pp 30−105. (c) Percec, V.; Tomazos, D. In *Comprehensive Polymer Science*; Aggarwal, S. L.; Russo, S., Eds.; Pergamon: Oxford, England, 1992; 1st Supplement; Chapter 14, pp 299−383.
(38) (a) Finkelmann, H. *Angew. Chem., Int. Ed. Engl.* **1987**, *26*, 816. (b) Hsu, C. S.; Percec, V. *Polym. Bull.* **1987**, *17*, 49. (c) Finkelmann, H.; Happ, M.; Portugall, M.; Ringsdorf, H. *Makromol. Chem.* **1978**, *179*, 2541.
(39) Magnini, P. *Makromol. Chem. Suppl.* **1981**, *4*, 223.
(40) (a) Imrie, C. T.; Karasz, F. E.; Attard, G. S. *Macromolecules* **1993**, *26*, 545. (b) Imrie, C. T. *Struct. Bonding* **1999**, *95*, 149.
(41) Griffin, A. C.; Sullivan, S. L.; Hughes, W. E. *Liq. Cryst.* **1995**, *18*, 851.
(42) Mariani, P.; Rustichelli, F.; Torquati, G. In *Physics of Liquid Crystalline Materials*; Khoo, I.-C., Simoni, F., Eds.; Gordon & Breach Science: New York, 1991; Chapter 1.

MA992097J